

# Hierarchy of bifurcations in the truncated and forced nonlinear Schrödinger model

Eli Shlizerman and Vered Rom-Kedar

*Faculty of Mathematical and Computer Science, Weizmann Institute, Rehovot 76100, Israel*

(Received 28 September 2004; accepted 11 October 2004; published online 28 January 2005)

The truncated forced nonlinear Schrödinger (NLS) model is known to mimic well the forced NLS solutions in the regime at which only one linearly unstable mode exists. Using a novel framework in which a hierarchy of bifurcations is constructed, we analyze this truncated model and provide insights regarding its global structure and the type of instabilities which appear in it. In particular, the significant role of the forcing frequency is revealed and it is shown that a parabolic resonance mechanism of instability arises in the relevant parameter regime of this model. Numerical experiments demonstrating the different types of chaotic motion which appear in the model are provided. © 2005 American Institute of Physics. [DOI: 10.1063/1.1831591]

**Putting an order in a multidimensional chaotic system by classifying all the different types of trajectories and finding their corresponding phase space regions is, in general, a formidable and perhaps even unattainable task. Near-integrable Hamiltonian systems are a fascinating playground in this respect as some rough classification may be found. Indeed, we demonstrate here that in some cases their structure may be well described via the construction of a three-level hierarchy of bifurcations. The analysis reveals, in a systematic way, the typical and singular solutions on a given energy level, and how these are altered as the energy level and the parameters are varied. In particular, all the different types of singular unperturbed solutions arising in a given model may be classified. The various types of chaotic trajectories which are produced by the perturbation in the neighborhood of such solutions are shown. The concrete system we analyze is a two-mode truncation of the forced one-dimensional nonlinear Schrödinger equation, an equation which describes many phenomena in physics such as the Bose–Einstein condensation. Our analysis explains the phase-space structure of this extensively studied reduced model, discloses the significance of the forcing frequency parameter, and reveals new types of chaotic solutions in it.**

## I. INTRODUCTION

The one-dimensional nonlinear Schrödinger (NLS) equation emerges as a first-order model in a variety of fields in physics—from high-intensity laser beam propagation to Bose–Einstein condensation to water waves theory; since it is the lowest order normal form for the propagation of strongly nonlinear dispersive waves its appearance in such a wide range of applications is mathematically obvious (see Ref. 1 and references therein). It was one of the triumphs of mathematics when it was realized that the NLS is completely integrable in one dimension on the infinite line (or with periodic boundary conditions) and hence completely solvable, leading to the beautiful theoretical development of inverse scattering, Lax pair, and spectral analysis of such nonlinear

systems.<sup>2</sup> The realization that such integrable structure might not persist under small perturbations led, almost two decades ago,<sup>3,4</sup> to the development of a program in which the influence of forcing and damping that breaks the integrability of the partial differential equation (PDE) is considered. This program included extensive numerical study of the perturbed PDEs which was presented in various forms. Since the phase space is infinite dimensional, it is indeed unclear which form supplies the best understanding of the solution's structure. It was then suggested that a finite-dimensional model—a two-mode Galerkin truncation of the perturbed NLS—faithfully describes the PDE dynamics when even and periodic boundary conditions are imposed and the  $L_2$  norm of the initial data is not too large.<sup>3–10</sup> Furthermore, it was shown that the unperturbed truncated system is a two degrees of freedom Hamiltonian system with an additional integral of motion, hence, is integrable. The study of the perturbed two-mode model is the main subject of this paper.

Previous investigation of the truncated system led to the discovery of a new mechanism of instability—the hyperbolic resonance—by which homoclinic solutions to a lower dimensional resonance zone are created.<sup>11–14</sup> The unperturbed structure of the truncated model which is responsible for this behavior is a circle of fixed points which is hyperbolic in the transverse direction (see Sec. III for a precise definition). New methodologies and tools introduced to this PDE-ODE study have finally led to a proof that the homoclinic resonance dynamics, and in particular the birth of new types of multipulse homoclinic orbits which is associated with it, has analogous behavior in the PDE setting (see Refs. 1, 10, 15, and 16, and references therein).

The appearance of a hyperbolic circle of fixed points in the truncated model is not a special property of the NLS model—investigation of the structure of low-dimensional near-integrable Hamiltonian systems (see Ref. 17) shows that hyperbolic resonances are a persistent phenomenon in  $n$  degrees of freedom systems with  $n \geq 2$ ; among such integrable Hamiltonian systems there are open sets of Hamiltonians which have an  $n-1$ -dimensional torus of fixed points which

is normally hyperbolic. The existence of such tori may be formulated as the existence of transverse intersection of some finite-dimensional manifolds. Hence, using the transversality theorem, one proves that hyperbolic resonant tori exist for a  $C^1$ -open set of integrable Hamiltonians, which we take hereafter as the definition of persistence.

The framework of studying the phase-space structure of the perturbed NLS and its modal truncations as perturbations to increasingly larger dimensional integrable systems appears to be promising. Yet, despite a century-long study of near-integrable Hamiltonian systems, our qualitative understanding of inherently higher dimensional (nonreducible to smooth, symplectic two-dimensional maps) near-integrable dynamics is lacking. Qualitative understanding means here that the effect of small perturbations on different unperturbed orbits may be *a priori* predicted for some nontrivial time scales. For example, such a qualitative understanding exists for generic near-integrable one-and-a-half degrees of freedom systems; the unperturbed periodic orbits which fill almost all of the phase space are replaced by KAM tori, Cantori, and resonance bands, whereas the neighborhood of homoclinic loops of the integrable system is replaced by homoclinic chaotic zones. While there are some long-standing open problems regarding the asymptotic behavior of such systems (notably the decay rate of averaged observables in the chaotic zone and the measure of the chaotic zone<sup>18,19</sup>), the basic transport and instability mechanisms are well understood on time scales which are logarithmic in the perturbation parameter.<sup>20,21</sup> Another example is the behavior of orbits of near-integrable  $n$  degrees of freedom (d.o.f.) systems in a neighborhood of an unperturbed, compact, regular non-degenerate level set with Diophantine frequency vector; while the asymptotic behavior of the solutions in such regions is still unknown (the famous Arnold diffusion conjecture), it is known that for extremely long time (at least exponential in the perturbation parameter<sup>22,23</sup>) the orbits will hover near the preserved KAM tori. In both examples, while the asymptotic behavior is unknown, there is a good understanding of the characteristic behavior of all orbits in a given neighborhood for a long transient time.

Here, we propose the following framework for obtaining such a qualitative information for a class of  $n$  d.o.f. near-integrable Hamiltonian systems (and demonstrate this approach on the truncated NLS equations). Given an integrable  $n$ -degrees of freedom family of Hamiltonian systems  $H_0(q, p; \mu)$  depending on the vector of parameters  $\mu$ , consider the following three-level hierarchy of bifurcations: The first stage consists of the analysis of the structure of the level sets (the sets of phase-space points along which all  $n$  constants of motion are fixed) on a single energy surface (the set of phase-space points along which the unperturbed energy is fixed). Bifurcation values at this level correspond to the values of the constants of motion across which the topology of the level sets on a given energy surface  $H_0(q, p; \mu) = h$  is changed. The set of these values was called the “bifurcation set” by Smale<sup>24</sup> and the “singularity manifolds” by Lerman and Umanskii.<sup>25</sup> The energy-momentum bifurcation diagram and the branched surfaces provide a complete description of this level set’s structure on any given energy surface. These

tools correspond to generalizations and extensions of the standard energy-momentum maps and the Fomenko graphs which were previously developed and applied to several interesting integrable systems.<sup>24–31</sup> These diagrams were constructed for a simple 2-d.o.f. model which describes the motion of high-altitude weather balloons in the atmosphere. In Refs. 17, 32, and 33 such diagrams were constructed for a variety of normal form-type models with  $n=2$  and 3. The main emphasis in these constructions is that, given a conservative perturbation, the Hamiltonian which is preserved in the perturbed flow defines the energy surfaces which are close, metrically but not necessarily topologically, under some mild conditions, to the perturbed surfaces (see Appendix A). Thus, the structure of the unperturbed surfaces supplies *a priori* bounds to the perturbed motion.

The next level in the hierarchy consists of the energy bifurcation values  $h^b$  across which the energy surfaces are no longer  $C^1$  conjugate. Thus, it describes how the energy surface differential topology is changed with  $h$ . This level of bifurcation was implicitly mentioned before<sup>24,29,31</sup> but has not been fully investigated. We have shown in Refs. 17, 32, and 33 that the energy-momentum bifurcation diagram supplies a graphical tool for realizing such bifurcation scenarios on this second level. In Refs. 17 and 32–35 we have shown that the simplest bifurcation (a fold in the codimension one singularity surfaces) is associated with resonances—namely with a dynamical phenomenon! Indeed, previous works have mostly concentrated on one specific dynamical phenomenon which changes the level set topology—the appearance of isolated fixed points, where the structure of the level sets and the energy surfaces becomes more complex as  $n$  increases (see Refs. 25, 29, and 36, and related works). Here, we list all the other *known* scenarios creating energy bifurcation values for the 2-d.o.f. case (folds, cusps and their symmetric analogs, curve crossings, and asymptotes to infinity) and discuss their dynamical implications (resonances, parabolicity, lower dimensional tori, *or* global bifurcations *or* no special local implications, unknown yet, respectively).

The last level in the hierarchy is concerned with the parameter dependence of the energy bifurcation values. The bifurcation values here are the parameter values  $\mu^b$  at which the bifurcation sequence of the second level changes (e.g., by changing the order of the energy bifurcating values). For example, for the 2-d.o.f. case, at a parameter value for which the fold-resonance energy bifurcation value  $h^{\text{res}}$  intersects the cusp-parabolic energy bifurcation value  $h^{\text{par}}$ , a resonant parabolic circle<sup>35</sup> (a circle of fixed points which is normally parabolic) is created. The perturbed motion near parabolic resonant tori exhibits instability. We establish here that a parabolic resonance appears for some relevant parameter values in the perturbed truncated NLS model, and demonstrate that the perturbed orbits near such values are of different characteristics than the trajectories which were previously observed. Using this framework the importance of a second parameter, the forcing frequency, which was set to be 1 in most previous studies, is highlighted.

The paper is ordered as follows: In Sec. II we describe the model which we study—the two-mode truncation of the forced NLS equation. In Sec. III we discuss the structure of

the perturbed and unperturbed energy surfaces, and in Sec. IV we construct the energy-momentum bifurcation diagram and the Fomenko graphs for this model. Together, these supply complete information on the structure of the energy surfaces and their dependence on the energy, namely this section completes the first level of the hierarchy of bifurcations analysis. In Sec. V we present numerical solutions of the perturbed model at regular energy values in various forms, demonstrating how the underlying integrable structure determines their character. Next, in Sec. VI we discuss the second level of the hierarchy—the energy bifurcation values. We show that in our model three possible mechanisms for the appearance of such bifurcations exist and for completeness we discuss one other mechanism which appears in other models. We demonstrate that the appearance of energy bifurcation values is usually associated with some dynamical phenomenon of the perturbed trajectories. Finally, in Sec. VII we describe how the energy bifurcation values vary with the model parameters—the interval length and the frequency of the forcing. We again relate parameter bifurcation values with dynamical phenomenon of the perturbed dynamics. After the discussion and the conclusions, in Appendix A, we prove that under quite general conditions on  $n$  d.o.f. systems, for small Hamiltonian perturbations, the energy surfaces of the perturbed and unperturbed systems are close to each other (yet not necessarily topologically conjugate). Appendix B consists of several energy-momentum bifurcation diagrams and their corresponding Fomenko graphs.

## II. THE NLS EQUATION

Consider the following forced and damped NLS equation:

$$-i\psi_T + \psi_{XX} + |\psi|^2\psi = i\varepsilon(\alpha\psi - \Lambda\psi_{XX} + \Gamma \exp(-i\Omega^2 T)), \quad (1)$$

with periodic boundary conditions and with even solutions in  $X$

$$\psi(X, T) = \psi(X + L, T), \psi_X(0, T) = 0.$$

Let

$$B = \psi \exp(i\Omega^2 T). \quad (2)$$

Then,  $B$  satisfies the same boundary conditions as  $\psi$  and the autonomous (time-independent) equation

$$-iB_T + B_{XX} + (|B|^2 - \Omega^2)B = i\varepsilon(\alpha B - \Lambda B_{XX} + \Gamma). \quad (3)$$

This equation was extensively studied in the last two decades,<sup>3–9</sup> and in this section we will mention only the relevant results. In this context, the perturbed NLS was first derived as a small amplitude envelope approximation of the damped driven sine-Gordon equation (SGE) when the driving force is in the near-resonance frequency. Then,  $\Omega=1$  and the only parameter appearing in the unperturbed system is the box size  $L$ .

The space of spatially uniform solutions  $[B(X, T) = (1/\sqrt{2})c(T)]$  is invariant under the perturbed flow (1) and the unperturbed solutions are of the form  $c(T)$

$=|c(0)|\exp(i(\Omega^2 - \frac{1}{2}|c(0)|^2)T + i\gamma(0))$ . Linear stability analysis of such solutions at  $\varepsilon=0$  shows that there is exactly one unstable mode,  $\cos(2\pi X/L)$ , when

$$\frac{2\pi}{L} < |c(0)| \leq \frac{4\pi}{L}, \quad (4)$$

whereas for lower values of  $|c(0)|$  the plane-wave solution is linearly stable (neutral). The various references use various rescalings of  $\psi$ ,  $X$ , and  $T$ , leading to some multiplication constants in the above relation—all of these relations are of course equivalent. Furthermore, in most of the works either  $L$  or  $\Omega$  (usually  $\Omega$ ) is considered as fixed. We see that for large box size the plane-wave solution is unstable even for small amplitude, as expected.

Consider a two-mode complex Fourier truncation for Eq. (3)

$$B_2(X, T) = \frac{1}{\sqrt{2}}c(T) + b(T)\cos kX, \quad (5)$$

where the periodic boundary conditions imply that

$$k = \frac{2\pi}{L}j, \quad j \in Z_+, \quad (6)$$

and since we are interested in the first unstable mode we take  $j=1$ . Substituting this solution to the NLS equation (3), setting  $\alpha=\Lambda=0$  and  $\Gamma=1$ , and neglecting (see Refs. 3–10 for discussion of this step) higher Fourier modes, we obtain the following equations of motion:

$$-i\dot{c} + \left(\frac{1}{2}|c|^2 + \frac{1}{2}|b|^2 - \Omega^2\right)c + \frac{1}{2}(cb^* + bc^*)b = i\sqrt{2}\varepsilon, \quad (7)$$

$$-i\dot{b} + \left(\frac{1}{2}|c|^2 + \frac{3}{4}|b|^2 - (\Omega^2 + k^2)\right)b + \frac{1}{2}(bc^* + cb^*)c = 0.$$

Here,  $|b|$  is the amplitude of the first symmetric mode and  $|c|/\sqrt{2}$  is the amplitude of the plane wave. These equations are of the form of a 2-degrees of freedom near-integrable Hamiltonian system with the Hamiltonian

$$H(c, c^*, b, b^*; \varepsilon) = H_0(c, c^*, b, b^*) + \varepsilon H_1(c, c^*, b, b^*), \quad (8)$$

and the Poisson brackets  $\{f, g\} = -2i(\langle \partial/\partial c, \partial/\partial c^* \rangle + \langle \partial/\partial b, \partial/\partial b^* \rangle)$ , where

$$H_0 = \frac{1}{8}|c|^4 + \frac{1}{2}|b|^2|c|^2 + \frac{3}{16}|b|^4 - \frac{1}{2}(\Omega^2 + k^2)|b|^2 - \frac{\Omega^2}{2}|c|^2 + \frac{1}{8}(b^2c^{*2} + b^{*2}c^2), \quad (9)$$

$$H_1 = \frac{-i}{\sqrt{2}}(c - c^*).$$

Furthermore, at  $\varepsilon=0$ , these equations possess an additional integral of motion

$$I = \frac{1}{2}(|c|^2 + |b|^2), \quad (10)$$

and thus are integrable; see Refs. 3, 4, and 8–10.

### III. ENERGY SURFACES

Here, the closeness of the perturbed and unperturbed energy surfaces is discussed, the expected structure of energy surfaces of 2-degrees-of-freedom integrable Hamiltonians is described, and finally the specific structure of the energy surfaces of the unperturbed truncated NLS model is found.

#### A. Perturbed energy surfaces

Most of this paper is devoted to the study of the structure of the energy surfaces of the integrable part of the truncated NLS model. Before we delve into this study, we notice that it supplies *a priori* bounds to the perturbed motion. Indeed, since the perturbation is Hamiltonian and *autonomous*, for any  $\varepsilon$ , a perturbed orbit with energy  $h$  [so  $H(c, b; \varepsilon) = h$ ,  $(c, b) \in \{c(t), b(t)\}_{t \in \mathbb{R}}$ ] satisfies  $H_0(\cdot) = h - \varepsilon H_1(\cdot; \varepsilon)$ . Notice the importance of the transformation (2) which transforms the nonautonomous equation (1) to the autonomous one (3), and the resulting dependence of the unperturbed equation on  $\Omega$ . We prove below that for small  $\varepsilon$ , points belonging to the perturbed and unperturbed energy surfaces must be close, uniformly in  $h$ , as long as  $\|\nabla H_0(\cdot)\|$  is bounded away from zero and the growth rate of  $H_1$  for large  $\|(c, b)\|$  is slower than that of  $H_0$ . Hereafter, all norms are the Euclidean norms:  $\|(q, p)\|^2 = \sum_{i=1}^n |q_i|^2 + \sum_{i=1}^n |p_i|^2$  and  $\|\nabla H\|^2 = \sum_{i=1}^n |\partial H / \partial q_i|^2 + \sum_{i=1}^n |\partial H / \partial p_i|^2$ . Hence, the structure of the unperturbed energy surfaces in an  $O(\varepsilon)$  interval of energies near  $h$  supplies global information on the allowed range of motion of the perturbed orbits. More precisely:

**Property 1.** *The Hamiltonian  $H(q, p; \varepsilon) = H_0(q, p) + \varepsilon H_1(q, p; \varepsilon)$  is said to have the boundness property if  $H_0(q, p)$  and  $H_1(q, p; \varepsilon)$  are  $C^\infty$  and are bounded with bounded derivatives on bounded sets. Moreover, for any  $L_2 > 0$  there exists a constant  $L_1$  and an  $\varepsilon_1$  such that for all  $0 \leq \varepsilon < \varepsilon_1$*

$$\|\nabla H_0(q, p)\|$$

$$> L_2 \max \left\{ \|\nabla H_1(q, p; \varepsilon)\|, \frac{|H_1(q, p; \varepsilon)|}{\|(q, p)\|}, \varepsilon \frac{\left| \frac{\partial H_1(q, p; \varepsilon)}{\partial \varepsilon} \right|}{\|(q, p)\|} \right\}$$

$$\text{for all } \|(q, p)\| > L_1. \tag{11}$$

**Theorem 1.** *Consider a near-integrable Hamiltonian  $H(q, p; \varepsilon) = H_0(q, p) + \varepsilon H_1(q, p; \varepsilon)$ ,  $\varepsilon \ll 1$ ,  $(q, p) \in M$ , where  $M$  is a  $2n$ -dimensional symplectic manifold and  $H$  satisfies the boundness Property 1. Consider the energy surface  $M^\varepsilon(h) = \{(q^\varepsilon, p^\varepsilon) | H(q^\varepsilon, p^\varepsilon; \varepsilon) = h\}$ . Then, for each  $\delta > 0$  there exists an  $\varepsilon_0(\delta)$  and a constant  $K(\delta)$  (independent of  $h$ ) such that for all  $0 \leq \varepsilon < \varepsilon_0(\delta)$ , and for all  $(q^\varepsilon, p^\varepsilon) \in M^\varepsilon(h)$  satisfying*

$$\|\nabla H_0(q^\varepsilon, p^\varepsilon)\| > \delta,$$

*there exists  $(q^0, p^0) \in M^0(h)$  [i.e.,  $H_0(q^0, p^0) = h$ ] such that  $\|(q^\varepsilon, p^\varepsilon) - (q^0, p^0)\| < K(\delta)\varepsilon$ .*

*Proof:* See Appendix A for details. First, we prove that since  $\|\nabla H_0(q^\varepsilon, p^\varepsilon)\|$  is bounded away from zero, so is  $\|\nabla H(q^\varepsilon, p^\varepsilon)\|$ . Then, an implicit function type of argument

shows that one can extend the solution of  $H(q^\varepsilon, p^\varepsilon; \varepsilon) = h$  from any given  $\varepsilon$  in the interval  $(0, \varepsilon_0(\delta))$  to zero—which completes the proof. Using the bounds of Property 1 allows one to show that this continuation may be done uniformly in  $\|(q, p)\|$ ; hence, it is independent of  $h$ . ■

The Hamiltonian (9) satisfies the theorem assumptions since  $H_0$  has quartic growth in  $|c|, |b|$ , whereas  $H_1$  is linear in  $|c|$ ; see Appendix A for more details. Therefore, we conclude that the perturbed and unperturbed energy surfaces are close to each other as long as the level sets belonging to the unperturbed energy surface are bounded away from neighborhoods of fixed points (where  $\nabla H_0$  vanishes). Since the fixed points of the system (7) belong to a finite number of level sets, hence they reside on a finite number of isolated energy surfaces (see Appendix A) and one concludes that for the most part of the phase space the unperturbed and perturbed surfaces are close to each other. The behavior near the fixed points requires further analysis, as expected.

Notice that the closeness of the perturbed and unperturbed energy surfaces *does not* imply that they are topologically conjugate. Nonetheless, this geometrical closeness is sufficient to obtain *a priori* bounds on the motion! Another point is that the Euclidean distance is clearly coordinate dependent, yet a smooth symplectic transformation of the coordinates will merely change the constant  $K(\delta)$  in the theorem.

#### B. The unperturbed energy surfaces

The integrable 2-d.o.f. truncated NLS Hamiltonian,  $H_0(c, b)$ ,  $(c, b) \in M = \mathbb{C} \times \mathbb{C}$ , has two integrals of motion:  $H_0$  and  $I$ . Both integrals are smooth functions of their variables, and they are pairwise in involution:  $\{H_0, I\} = 0$ . Furthermore, since the level sets of  $I$ , in the  $(c, b)$  4-dimensional space, are 3-spheres, the Hamiltonian level sets  $M_g = \{(c, b) \in M, H_0(c, b) = g_1, I(c, b) = g_2\}$ , are clearly compact; hence, the unperturbed flow is complete. By the Liouville–Arnold theorem (see Refs. 27, 37, and 38), the connected compact components of the level sets  $M_g$ , on which  $dI$  and  $dH_0$  are (pointwise) linearly independent, are diffeomorphic to 2-tori, and hence a transformation to action-angle coordinates [ $H_0 = H_0(J)$ ] near such level sets is nonsingular. Here, direct computation shows that  $dI$  and  $dH_0$  are linearly independent for almost all values of  $c$  and  $b$ .

Consider a neighborhood of a level set  $M_{g_0}$  which contains a singularity set at which  $dI$  and  $dH_0$  are linearly dependent (e.g., the plane  $c=0$ ), but do not vanish simultaneously. Then, on each connected and closed component of such a Hamiltonian level set there is some neighborhood  $D$ , in which the Hamiltonian  $H_0(c, b)$  may be transformed by the reduction procedure to the form (see Refs. 25 and 37)

$$H_0(\bar{q}, \bar{p}, J), \quad (\bar{q}, \bar{p}, \phi, J) \in U \subseteq \mathbb{R}^1 \times \mathbb{R}^1 \times \mathbb{T}^1 \times \mathbb{R}^1, \tag{12}$$

which does not depend on the angles of the torus,  $\phi$ . The symplectic structure of the new integrable Hamiltonian (12) is  $d\bar{q} \wedge d\bar{p} + d\phi \wedge dJ$ , where  $(\bar{q}, \bar{p}, \phi, J)$  are the generalized action-angle variables.

TABLE I. Singular circles.

Invariant circle: $\theta, \gamma \in T^1$	Exists for	Description
(1) $p_{pw}=(x=0, y=0, I, \gamma)$ ,	$I \geq 0$	Plane wave ( $b=0$ )
(2) $p_{sm}=(u=0, v=0, I, \theta)$ ,	$I \geq 0$	Symmetric mode ( $c=0$ )
(3) $p_{pwm}^\pm =$ $(x = \pm \sqrt{\frac{4}{7}(-k^2 + 2I)}, y = 0, I, \gamma)$ , $(u = \pm \sqrt{\frac{6}{7}I + \frac{4}{7}k^2}, v = 0, I, \theta)$ ,	$I \geq \frac{1}{2}k^2$ $I > \frac{1}{2}k^2$	PW mixed mode ( $bc \neq 0$ ) "
(4) $p_{smm}^\pm =$ $(x = 0, y = \pm 2k, I, \gamma)$ , $(u = 0, v = \pm \sqrt{2I - 4k^2}, I, \theta)$ ,	$I > 2k^2$ $I \geq 2k^2$	SM mixed mode ( $bc \neq 0$ ) "

For our model, the symmetry  $c \rightarrow c \exp(i\gamma)$ ,  $b \rightarrow b \exp(i\gamma)$  of  $H_0(c, b)$  inspired the following symplectic change of variables to the generalized action angle coordinates  $(x, y, I, \gamma)$  (see Ref. 14):

$$c = |c| \exp(i\gamma), \quad b = (x + iy) \exp(i\gamma), \tag{13}$$

$$I = \frac{1}{2}(|c|^2 + x^2 + y^2). \tag{14}$$

Then, the Hamiltonian (9) becomes

$$H(x, y, I, \gamma) = H_0(x, y, I) + \varepsilon H_1(x, y, I, \gamma),$$

where

$$(I, \gamma) \in (R^+ \times T), \quad (x, y) \in B_I = \{(x, y) | x^2 + y^2 < 2I\},$$

and

$$H_0(x, y, I) = \frac{1}{2}I^2 - \Omega^2 I + (I - \frac{1}{2}k^2)x^2 - \frac{7}{16}x^4 - \frac{3}{8}x^2y^2 + \frac{1}{16}y^4 - \frac{1}{2}k^2y^2, \tag{15}$$

$$H_1(x, y, I, \gamma) = \sqrt{2} \sqrt{2I - x^2 - y^2} \sin \gamma. \tag{16}$$

The transformation to these variables is singular at  $c=0$ , namely on the circle  $2I=x^2+y^2$ , where the phase  $\gamma$  is ill defined and the perturbation term has a singular derivative. In previous works<sup>11-14</sup> the analysis was performed for phase-space regions which are bounded away from this circle. We introduce a similar symplectic transformation which is valid as long as  $b \neq 0$

$$b = |b|e^{i\theta}, \quad c = (u + iv)e^{i\theta}, \quad I = \frac{1}{2}(u^2 + v^2 + |b|^2), \tag{17}$$

and obtain the equation of motion in the canonical coordinates  $(u, v, I, \theta)$  from the Hamiltonian (9)

$$H_0(u, v, I) = \frac{3}{4}I^2 + (-\Omega^2 + \frac{3}{4}u^2 - \frac{1}{4}v^2 - k^2)I - \frac{7}{16}u^4 - \frac{3}{8}u^2v^2 + \frac{1}{2}k^2u^2 + \frac{1}{2}k^2v^2 + \frac{1}{16}v^4,$$

$$H_1(u, v, I) = \sqrt{2}(v \cos \theta + u \sin \theta).$$

When both  $\gamma$  and  $\theta$  are well defined [the  $(x, y, I, \gamma)$  and the  $(u, v, I, \theta)$  correspond to two charts of the 3-sphere defined by Ref. 39], namely for  $cb \neq 0$ , the two sets of coordinates are simply related

$$x = |b| \cos(\theta - \gamma), \quad y = |b| \sin(\theta - \gamma),$$

$$u = \frac{|c|}{|b|}x, \quad v = -\frac{|c|}{|b|}y.$$

The geometrical structure of the new Hamiltonian,  $H_0(\bar{q}, \bar{p}, J)$ , is such that for any fixed  $J$  a circle is attached to every point of the  $(\bar{q}, \bar{p})$  plane. The singular level sets contain a fixed point in the normal plane  $(\bar{q}, \bar{p})$

$$\nabla_{(\bar{q}, \bar{p})} H_0(\bar{q}, \bar{p}, J)|_{p_f} = 0, \quad p_f = (\bar{q}_f, \bar{p}_f, J_f). \tag{18}$$

Generically, for 2-degrees-of-freedom systems, we expect to have a one-parameter family of solutions to these equations, namely a one-parameter family of circles  $(\bar{q}_f, \bar{p}_f, J_f, \phi)$ . The stability type of these circles in the normal direction to the family of circles is simply determined by the stability of the fixed points of the reduced system (the system in the normal plane<sup>27,39,40</sup>), which, in the  $(\bar{q}, \bar{p}, J)$  coordinate system is determined by

$$\det \left( \frac{\partial^2 H_0}{\partial^2 (\bar{q}, \bar{p})} \Big|_{p_f} \right) = -\lambda_{p_f}^2 \tag{19}$$

where  $p_f$  satisfies (18). Notice that a single circle belonging to this family has neutral stability in the action direction. The normal stability referred to in the Hamiltonian context ignores this direction; see Refs. 39 and 41 and references therein. When  $\lambda_{p_f}$  is real and nonvanishing the corresponding family of tori is said to be normally hyperbolic, when it vanishes it is called normally parabolic, and when it is pure imaginary it is normally elliptic; see the detailed references in Ref. 33 and the discussion in Ref. 39. The motion on these circles is described by the equations

$$\frac{d\phi}{dt} = \omega(\bar{q}_f, \bar{p}_f, J_f), \quad \frac{dJ}{dt} = 0,$$

where  $\omega(\bar{q}, \bar{p}, J) = [\partial H_0(\bar{q}, \bar{p}, J)] / \partial J$  is the frequency vector. Following the terminology of Ref. 25, the invariant circles on which Eq. (18) is satisfied are called here singular circles, and the curves of energy and action values on which this equation is satisfied [i.e., the curve  $(H_0(\bar{q}_f, \bar{p}_f, J_f), J_f)$  in the  $(H, J)$  plane] are called the singularity surfaces. We will see that the structure of these singularity surfaces serves as an organizing skeleton of the energy surfaces.

For our model, the singular circles are easily found by setting  $\nabla_{(x,y)} H_0(x, y, I) = 0$  for circles satisfying  $x^2 + y^2 < 2I$ , and similarly  $\nabla_{(u,v)} H_0(u, v, I) = 0$  for circles satisfying  $u^2 + v^2 < 2I$ . As in Refs. 11-14, we identify six such families of

TABLE II. Normal stability of singular circles.

Jacobian eigenvalues	Elliptic for	Hyperbolic for	Parabolic for
(1) $(\lambda_{pw})^2 = k^2(-k^2 + 2I)$	$I < \frac{1}{2}k^2$	$I > \frac{1}{2}k^2$	$I_p^{pw} = \frac{1}{2}k^2$
(2) $(\lambda_{sm})^2 = (\frac{3}{2}I + k^2)(\frac{1}{2}I - k^2)$	$I < 2k^2$	$I > 2k^2$	$I_p^{sm} = 2k^2$
(3) $(\lambda_{pwm})^2 = \frac{4}{7}(2k^4 - k^2I - 6I^2)$	$I > \frac{1}{2}k^2$	...	$I_p^{pw} = \frac{1}{2}k^2$
(4) $(\lambda_{smm})^2 = 4k^2(2k^2 - I)$	$I > 2k^2$	...	$I_p^{sm} = 2k^2$

singular circles as summarized in Table I—the plane-wave ( $b=0$ ) and symmetric mode ( $c=0$ ) families are the two pure states and the other four families correspond to circles which bifurcate from these two pure families when they lose stability.

Table II includes the calculation of the normal stability multipliers for these families of circles, namely the calculation of Eq. (19) for this case, showing that the first two families become unstable when their norm is increased above a threshold level which depends on the box size.

**Remark 1.** Recall that we expect the two-mode model to apply for regions in which the plane-wave solution has at most one unstable mode. Using (4) and (13), it follows that near the circle  $b=0$  we should expect the analysis to be valid for  $I \leq 2k^2$ . Interestingly enough, we see that exactly at this  $I$  value the symmetric mode solutions lose their stability. The analysis and numerical simulations of the truncated model with  $I > 2k^2$  are performed here to demonstrate some interesting dynamical phenomena, but their relevance to the full PDE dynamics is admittedly doubtful.

The dynamics in the angle direction for  $x^2 + y^2 < 2I$  is described by

$$\frac{d\gamma}{dt} = \omega(x, y, I) = I - \Omega^2 + x^2 = \frac{\partial H_0(x, y, I)}{\partial I}, \tag{20}$$

and for  $u^2 + v^2 < 2I$  we have

$$\frac{d\theta}{dt} = \omega(u, v, I) = \frac{3}{2}I - \Omega^2 + \frac{3}{4}u^2 - \frac{1}{4}v^2 - k^2 = \frac{\partial H_0(u, v, I)}{\partial I}. \tag{21}$$

In particular, the invariant circles listed in Table I have an inner frequency,  $\omega(I) = [\partial H_0(p_f)] / \partial I$ , and they correspond to

a circle of fixed points when this frequency vanishes as listed in Table III below.

Using the transformation to the  $(x, y, I)$  coordinates, the corresponding 2-d.o.f. system with  $\Omega=1$  was studied in the dissipative and conservative cases.<sup>1,11-14</sup> In particular, it was realized that a specially interesting phenomena occurs when the circle corresponding to a plane wave ( $b=0$ ) is a normally hyperbolic circle of fixed points (from Tables II and III and remark 1 we conclude that such a circle appears in the relevant regime for any  $\Omega$ , at  $I=\Omega^2$  for  $\Omega/\sqrt{2} < k < \sqrt{2}\Omega$ ). Then, at  $\varepsilon=0$ , pairs of fixed points on this circle are connected by two heteroclinic orbits. This realization led to a beautiful theoretical study of the behavior of integrable systems with such a normally hyperbolic circle of fixed points under conservative<sup>1,12,13</sup> and dissipative<sup>11,14</sup> perturbations, showing that the perturbed system has various types of homoclinic and heteroclinic orbits. Furthermore, these studies led to the development of a geometrical PDE approach by which it was proved that the perturbed NLS equation has homoclinic solutions to the resonant plane-wave solutions; see Refs. 1, 15, and 16, and references therein.

Kovacic<sup>14</sup> includes in his study global analysis of the integrable system in which, after identifying the critical  $I$  values, the level sets  $H=h$  are plotted for typical values of  $I$ . Here, we present the integrable system using energy-momentum bifurcation diagrams and Fomenko graphs, investigating the surfaces  $H=h$  and their extent in the  $I$  direction. This representation allows a better understanding of the behavior under small conservative perturbations since the total energy  $H$  is preserved. The implications of this representation on the damped case will be studied elsewhere.

TABLE III. Resonant and parabolic singular circles.

$\omega(p_f) = [dH(p_f)/dI]$	I-resonance	I-parabolic	Parabolic resonance
(1) $\omega^{pw} = I - \Omega^2$	$I_r^{pw} = \Omega^2$	$I_p^{pw} = \frac{1}{2}k^2$	$\Omega_{pr-pw} = \frac{1}{\sqrt{2}}k$
(2) $\omega^{sm} = \frac{3}{2}I - (k^2 + \Omega^2)$	$I_r^{sm} = \frac{2(\Omega^2 + k^2)}{3}$	$I_p^{sm} = 2k^2$	$\Omega_{pr-sm} = \sqrt{2}k$
(3) $\Omega^{pwm} = \frac{15}{17}I - \Omega^2 - \frac{4}{7}k^2$	$I_r^{pwm} = \frac{7\Omega^2 + 4k^2}{15}$	$I_p^{pw} = \frac{1}{2}k^2$	$\Omega_{pr-pw} = \frac{1}{\sqrt{2}}k$
(4) $\omega^{smm} = I - \Omega^2$	$I_r^{smm} = \Omega^2$	$I_p^{sm} = 2k^2$	$\Omega_{pr-sm} = \sqrt{2}k$

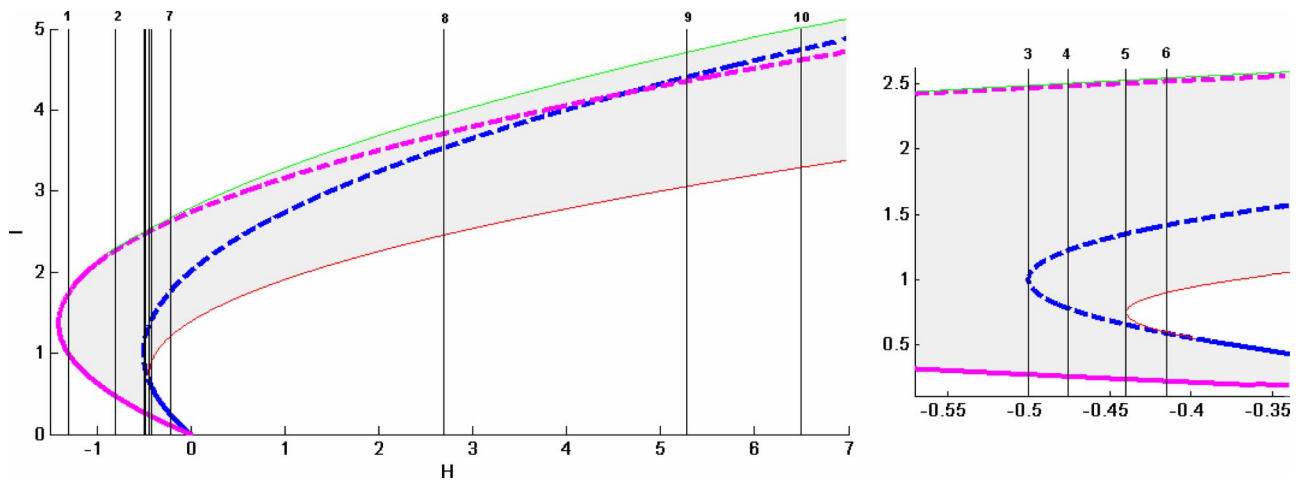


FIG. 1. (Color online). EMBD graph for  $k=1.025$ ,  $\Omega=1$ . Thick black (blue) line— $p_{pw}$ ; thin black (red) line— $p_{pwm}$ ; thick gray (magenta) line— $p_{sm}$ ; thin gray (green) line— $p_{smm}$ . Dashed lines—normally hyperbolic circles; solid lines—normally elliptic circles.

#### IV. ENERGY MOMENTUM BIFURCATION DIAGRAMS

The *energy-momentum bifurcation diagram (EMBD)* supplies global information on the bifurcations of the energy surfaces structure and their relation to resonances. Consider an integrable Hamiltonian system  $H_0(q, p)$  in a region  $D \subseteq M$  at which a transformation to the local generalized coordinate system  $H_0(\bar{q}, \bar{p}, J)$  is nonsingular. The energy-momentum map assigns to each point of the phase space  $(\bar{q}, \bar{p}, J)$  a point in the energy-momentum space  $(h=H_0(\bar{q}, \bar{p}, J), J)$ . The energy-momentum bifurcation diagram is a plot in the  $(h, J)$  space (for  $(h, J)$  in the range of  $D$ ) which includes (see Ref. 33 for the  $n$ -d.o.f. formulation)

- The region(s) of allowed motion (the closure of all regions in which the energy-momentum mapping is a trivial fiber bundle; see Refs. 24 and 27).
- The singular surfaces  $(h, J)=(H_0(p_f), J_f)$  [see Eq. (18)] where the normal stability of the corresponding singular circles, defined by Eq. (19), is indicated.
- The strongest resonance surfaces on which the inner frequency of the circles vanishes,  $\omega(p_f)=0$  {and possibly the regions in which backflow occurs, where  $[d\phi(\bar{q}, \bar{p}, J)]/dt$  changes sign along the level set  $(h=H_0(\bar{q}, \bar{p}, J), J)$ .
- The energies at which topological bifurcations occur and the Fomenko graphs in the intervals separated by these bifurcation points.

Note that the energy-momentum bifurcation diagram depends on the choice of the generalized action-angle coordinates  $(\bar{q}, \bar{p}, J)$ ; see Ref. 33 for discussion. In particular, *the form of the perturbation* determines the strongest resonant directions, and the actions in the EMBD are chosen accordingly. Here, Eq. (9) implies that the dominant resonant direction is indeed the conjugate angle to  $I$ , in both the  $(x, y, I)$  and the  $(u, v, I)$  coordinate systems. Hence, the convenient coordinates for the energy-momentum bifurcation diagram is  $(h, I)$ . Notice that while the momentum variable  $I$  is globally defined, the associated angle coordinate is defined differently near the plane-wave circles ( $b=0$ ) and near the symmetric

mode circles ( $c=0$ ). The EMBD contains the resonance information for both representations.

##### A. Construction of the EMBD

Calculation of the singular surfaces and the normal stability of the lower dimensional tori are the first steps in depicting the global structure of the energy surfaces. We begin the construction of the EMBD by plotting the singular surfaces  $(H_0(p_f(I)), I)$  in the  $(h, I)$  plane, where  $(p_f(I))$  are given by the six families of Table I.

In Fig. 1 we plot these curves for the nondimensional wave number  $k=1.025$  at  $\Omega=1$ , which is the value used in previous works.<sup>3,5-9</sup> Other values of  $k$  and  $\Omega$  are presented in Appendix B. We use the usual convention in bifurcation diagrams by which normally stable circles are denoted by solid lines, whereas normally hyperbolic circles are denoted by dashed lines (see Table II). Different colors are used for the different families of invariant circles [thick and thin black lines (blue and red in the color plots) for the plane wave and its bifurcating branch, and thick and thin gray lines (magenta and green in the color plots) for the symmetric mode and its bifurcation branch]. The allowed region of motion is shaded—for each point  $(h, I)$  in this shaded region there are  $(c, b)$  values satisfying  $H_0(c, b)=h$ ,  $I=\frac{1}{2}(|c|^2+|b|^2)$ . An energy surface in this diagram is represented by the intersection of a vertical line with the allowed region of motion. The topology of the level sets for different  $I$  values on a given energy surface [i.e., the number of disconnected 2-tori which correspond to each  $(h, I)$  value and the manner by which these tori glue together at the singular values] is represented by the Fomenko graphs as described next.

##### B. Fomenko graphs

The Fomenko graphs are constructed by assigning to each connected component of the level sets (on the given energy surface) a point on the graph, so there is a one-to-one correspondence between them (see Refs. 29 and 33). Then,

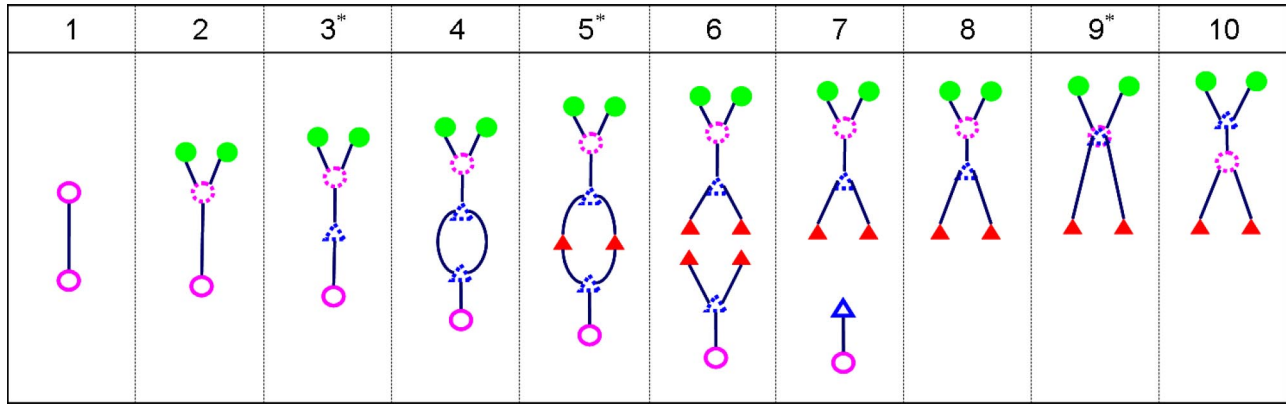


FIG. 2. (Color online). Fomenko graphs for  $k=1.025$ ,  $\Omega=1$ . Clear triangle— $p_{pw}$ ; solid triangle— $p_{pwm}$ . Clear circle— $p_{sm}$ ; solid circle— $p_{smm}$ .

an edge of this graph corresponds to a regular one-parameter family of two tori, whereas vertices correspond to singular values of  $(h, I)$  at which some families of tori glue together or shrink to a singular circle. In the standard construction of the Fomenko graphs<sup>29</sup> the main objective is the study of the topology of the surfaces and the level sets; hence, for example, all the normally elliptic singular circles are assigned the same symbol (molecule “A”). Here, we distinguish between the different singular circles as these correspond to different dynamic in the NLS. Thus, we denote the invariant circles corresponding to the plane-wave family ( $p_{pw}$ ) and the invariant circles which emanate from them ( $p_{pwm}^\pm$ ) by open and full triangles, respectively. The invariant circles corresponding to the symmetric mode family ( $p_{sm}$ ) and the invariant circles which emanate from them ( $p_{smm}^\pm$ ) are denoted by open and full circles. In this way the topological changes of the level sets are discovered and the energy surface may be reconstructed from these graphs.

Figure 1 shows the energy-momentum bifurcation diagram for the truncated NLS model at  $k=1.025$ ,  $\Omega=1$ . The numbered vertical lines on this figure indicate energy values for which the Fomenko graphs were constructed, as shown in Fig. 2. Thus, the simple segment corresponding to graph 1 in Fig. 2 corresponds to an  $S^2 \times S^1$  energy surface—a sphere in the  $(u, v, I)$  space, multiplied by the circle  $\theta \in S^1$ . Figure 3

shows the more complex energy surface at the energy level corresponding to line 5 in Fig. 1 and to diagram 5 in Fig. 2. Projections of the energy surface are plotted twice; the energy surface is the two-dimensional surface in the  $(x, y, I)$  space [respectively,  $(u, v, I)$  space] multiplied, for all  $c \neq 0$  (for all  $b \neq 0$ ), by the circle  $\gamma \in S^1$  ( $\theta \in S^1$ ). The redundant presentation in the  $(u, v, I)$  space is shown to better explain the level set’s topology near the circle  $c=0$ , where the transformation to the  $(x, y, I)$  coordinates is singular. In Fig. 3 we demonstrate more precisely the relations between the energy-momentum bifurcation diagram, the Fomenko graph, and the energy surface; indeed, let us describe in details the level set’s topology on this energy surface as the action  $I$  is increased.

- (1) The lowest  $I$  value corresponds to the intersection of line 5 with the solid gray line in Fig. 1, to the open circle on the Fomenko graph, and to the lowest level set in Fig. 3—the symmetric mode circle. The level set here is the circle  $c=0$ ,  $|b|=\sqrt{2I_{sm}}$ , which is normally elliptic. It is represented in the  $(u, v)$  plane as a point—the origin—which is multiplied by the circle in  $\theta$  [the representation in the  $(x, y)$  plane is singular here]. For a bit larger  $I$  values each level set is composed of one torus—the Fomenko graph has a single edge for such values of  $I$ , and

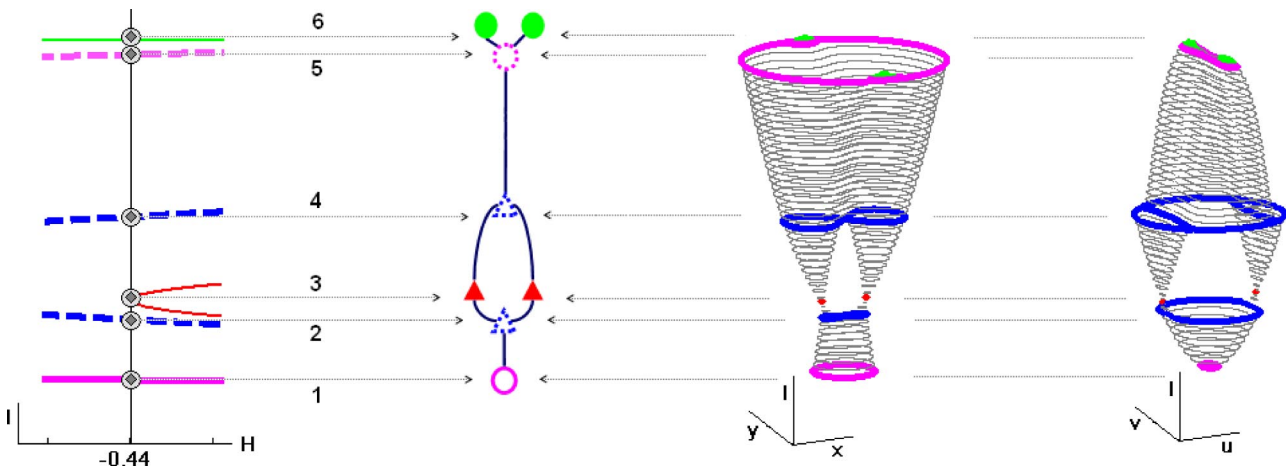


FIG. 3. (Color online). EMBD, Fomenko graph, and energy surfaces (mode  $S^1$ ) for  $k=1.025$ ,  $\Omega=1$ ,  $h=-0.44$ .

indeed we see that in both the  $(x, y)$  plane and the  $(u, v)$  plane a single circle, corresponding to a torus, appears.

- (2) When the  $I$  value reaches the dashed black line in Fig. 1, the level set becomes singular—it is composed of the plane-wave circle and its homoclinic surfaces, shown as a figure-eight level set in the  $(x, y)$  plane. On the three-dimensional energy surface this figure eight is multiplied by the circle  $\gamma \in S^1$ . This singular level set is denoted by the open triangle with dashed boundary in the Fomenko graph.
- (3) As  $I$  is further increased, each point in the  $(h, I)$  plane has two tori associated with it—in the Fomenko graph we see that there are two edges for these values of  $I$ , and the corresponding level sets at the  $(x, y)$  plane have two disconnected circles. These circles shrink to two points which are two normally elliptic invariant circles of the plane-wave-mixed-mode type at a critical  $I$  value at which line 5 is tangent to the curve corresponding to  $p_{pwm}$  in Fig. 1; for energies above line 5 the energy surface splits in two due to this curve. Thus, this value of the energy is an energy bifurcation value—the level sets for lower energies (diagram 4) and higher energies (diagram 6) undergo different topological changes as the action is increased along the energy surface (graphs corresponding to such energy bifurcation values are denoted here by \* in the Fomenko graph sequences). The two circles  $p_{pwm}^\pm$  are denoted by the solid triangles in the Fomenko graph.
- (4) Further increase of  $I$  leads us again to the two-tori situation until the curve  $p_{pw}$  is intersected again. Then, the two tori coalesce at the singular level set of the plane wave and its homoclinics, which is denoted as before by an open triangle.
- (5) Further increase of  $I$  leaves us with one connected component of the level sets until the dashed gray line in the EMBD, which denotes the normally hyperbolic circles  $p_{sm}$ , denoted in the Fomenko graph by an open circle, is intersected. This singular level set is again, topologically, a figure-eight times a circle, but now it is represented in the  $u, v$  plane [since the  $(x, y)$  coordinates are singular here].
- (6) For larger  $I$  values, in the Fomenko graph, two edges emanate from the circle corresponding to  $p_{sm}$ . These correspond to the two families of tori which oscillate near the two symmetric-mode-mixed-mode circles. The upper boundary of the energy surface is reached when these two tori shrink to the corresponding invariant circles—when line 5 intersected the thin gray line—when the two solid circles in the Fomenko graph are reached.

This rather lengthy explanation can be repeated now for each Fomenko graph without the explicit computation of the corresponding energy surfaces. Namely, these graphs encode all needed information for the reconstruction of the energy surfaces.<sup>29</sup> We note that a similar construction for some  $n$ -d.o.f. systems has been recently suggested (see Ref. 33 and references therein).

## V. THE NLS TRUNCATED SOLUTION'S STRUCTURE AT REGULAR ENERGY LEVELS

Using the EMBD and the Fomenko graphs, we gave a full description of the structure of the unperturbed solutions on a given energy surface in the  $(x, y, I, \gamma)$  and  $(u, v, I, \theta)$  coordinate system. An energy surface is a regular surface if the Fomenko graph is identical in its neighborhood<sup>31</sup> (e.g., in Fig. 2, graphs 1, 2, 4, 6, 7, 8, and 10 all correspond to regular values). For such energy values, the detailed understanding of the unperturbed structure immediately translates into a qualitative understanding of the perturbed motion: for sufficiently small perturbation an edge in the Fomenko graph (corresponding to a family of two tori) disintegrates into a Cantor set of KAM tori and Cantori with resonance bands (with their own chaotic zones) residing in the gaps of the Cantor set. The vertices which correspond to hyperbolic circles develop (generically) into circles with split separatrices with the usual chaotic zone associated with them. The vertices which correspond to normally elliptic circles have again the usual Birkhoff normal form/resonant behavior depending on the ratio of their normal and inner frequencies, which needs to be calculated. In Fig. 4 we show several perturbed orbits for  $h \approx -0.42$ , i.e., energy surface which is described by graph 6 in Fig. 2. To make the perturbed motions visible we let the  $\varepsilon$  value be 10 times larger than the  $\varepsilon$  value in the consequent figures of the perturbed orbits. Notice that this graph has eight different edges corresponding to eight separate families of two tori, three vertices corresponding to hyperbolic circles with separatrices, and seven vertices corresponding to normally elliptic circles.

The relation between the solutions in the  $(x, y, I, \gamma)$  [or  $(u, v, I, \theta)$ ] spaces to the truncated solution  $B_2(X, T)$  and hence to the truncated solution  $\psi_2(X, T) = B_2(X, T) \times \exp(-i\Omega^2 T)$  of Eq. (1) is easily found for  $c \neq 0$  via the transformations<sup>5,10</sup>

$$B_2(X, T) = \left( \sqrt{I(T) - \frac{1}{2}(x^2(T) + y^2(T))} + (x(T) + iy(T)) \cos kX \right) \exp(i\gamma(T)),$$

$$\psi_2(X, T) = B_2(X, T) \exp(-i\Omega^2 T),$$

and similarly for  $b \neq 0$

$$B_2(X, T) = \left( u(T) + iv(T) + \sqrt{I(T) - \frac{1}{2}(u^2(T) + v^2(T))} \cos kX \right) \exp(i\theta(T)),$$

$$\psi_2(X, T) = B_2(X, T) \exp(-i\Omega^2 T).$$

In previous works it was suggested that plots of  $|B(X, T)|$  as a function of  $(X, T)$  for a small interval of time (we will call this representation *the amplitude plot*) and a plot of  $(\text{Re}\{B(0, T)\}, \text{Im}\{B(0, T)\})$  for a longer  $T$  interval (we will call this representation *the B-plane plot*) reveal the difference between regular and chaotic motion. We present the various perturbed orbits which reside on the same energy surface in these projections. It is seen that left and right branches of tori with the same  $I$  values (oscillating near the circles  $p_{pwm}^+$  and  $p_{pwm}^-$ , respectively) appear in the  $B$ -plane plots as projections of tori with different radii (observe the light and dark green

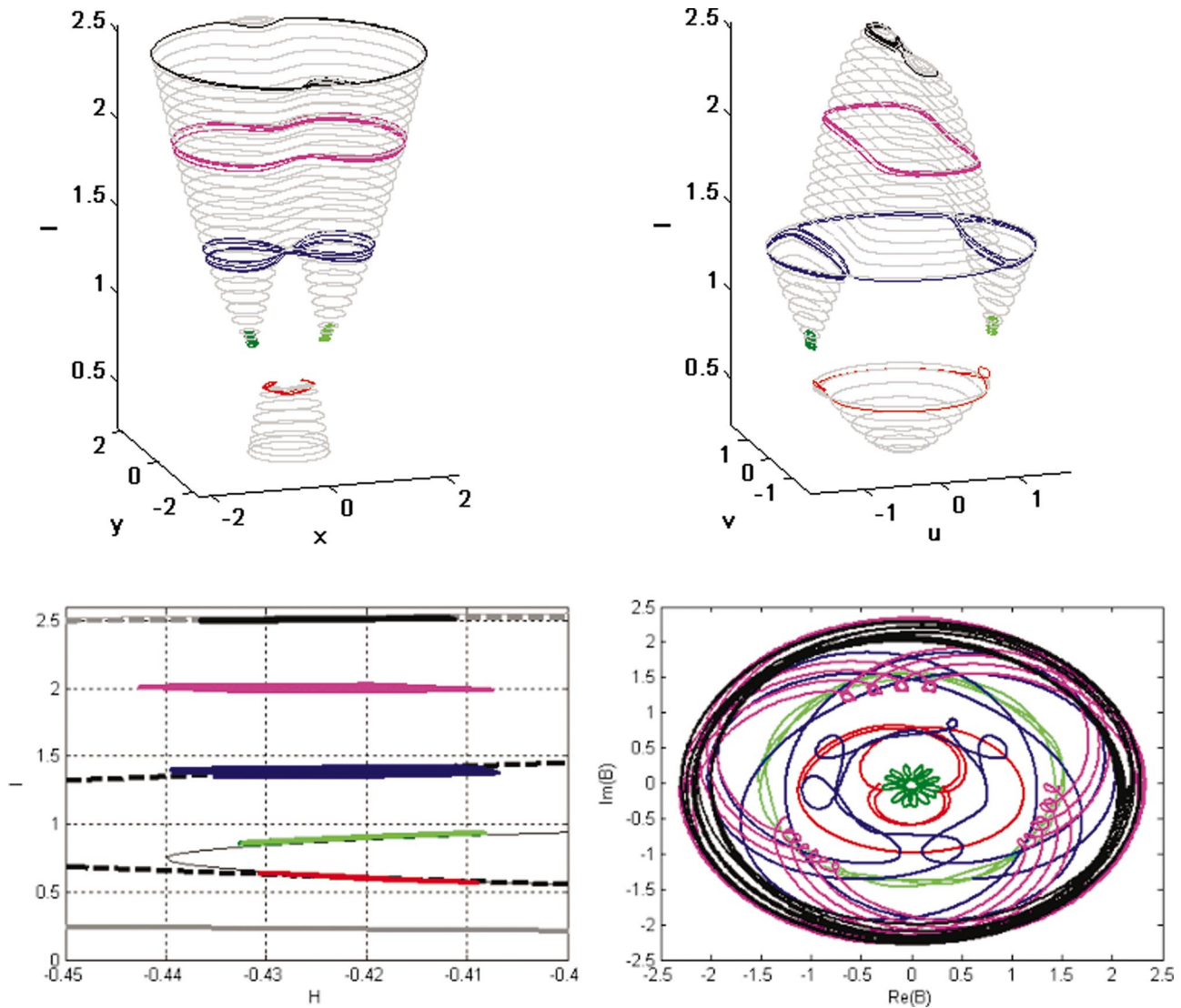


FIG. 4. (Color). Perturbed orbits on energy surface 6 shown on the projected energy surfaces, the EMBD, and the  $B$ -plane plot for  $\epsilon=(1/\sqrt{2})10^{-2}$ ,  $k=1.025$ ,  $h=-0.42$ .

orbits in Fig. 4), and in the amplitude plots as phase-shifted in  $X$  solutions (thus, the right branch has its maxima at  $X=0$ , whereas the left one at  $X=\pi/2k$ , as was demonstrated in the earlier works<sup>9</sup>). On the other hand, the upper and lower branches (oscillating near the circles  $p_{smm}^+$  and  $p_{smm}^-$ , respectively) are indistinguishable in these plots. Presenting  $\text{Re}\{B(X, T)\}$  for these solutions shows similar center-wings jumps. The chaotic solutions in these projections are shown as well, the ones associated with  $p_{pw}$  exhibiting left-right jumps in the amplitude plots and inner-outer radii jumps in the  $B$  plane plots, whereas the ones associated with  $p_{sm}$  show left-right jumps in the real  $B$  plots.

## VI. BIFURCATING ENERGY VALUES

Intersecting the energy-momentum bifurcation diagrams with a vertical line and constructing the corresponding Fomenko graphs leads to a full description of a given energy surface. It follows that changes in the differential topology of the energy surfaces can be easily read off from these diagrams—they precisely correspond to singularities of the

singularity curves (the curves corresponding to the circles in the EMBD) with respect to changes in the energy, namely to folds, branchings (cusps), intersections, and asymptotes of the singularity curves to a vertical line. The dynamical phenomena associated with each of these simplest geometrical features of the singularity surfaces are listed below. Thus, for the 2-degrees-of-freedom case singularity theory may be used to classify all possible energy bifurcation values (see also Ref. 33). Here, we do extend some of the notions to the  $n$ -d.o.f. framework as this has not been previously discussed. A complete classification of all the possible singularities of these singularity surfaces and their dynamical consequences has not been developed yet.

### A. Folds in the singularity surfaces and resonances

Clearly (see, for example, Fig. 1), the energy surfaces change their topology whenever there is a fold in the singularity surfaces. Furthermore, it was established in Ref. 33

TABLE IV. Singular surfaces—Hamiltonian at the singular circles.

$H_0(x_f, y_f, I)$ Evaluation	Exist for
(1) $H(x_{pw}, y_{pw}, I) = H(0, 0, I) = \left(\frac{I^2}{2} - \Omega^2 I\right)$	$I \geq 0$
(2) $H(u_{sm}, v_{sm}, I) = (0, 0, I) = \frac{3}{4}I^2 - I(\Omega^2 + k^2)$	$I \geq 0$
(3) $H(x_{pwm}^\pm, y_{pwm}^\pm, I) = \frac{15}{14}I^2 - (\Omega^2 + \frac{4}{7}k^2)I + \frac{1}{7}k^4$	$I \geq \frac{1}{2}k^2$
(4) $H(u_{smm}^\pm, v_{smm}^\pm, I) = \frac{I^2}{2} - \Omega^2 I - k^4$	$I \geq 2k^2$

that extremum of nonparabolic singularity surfaces correspond to strong resonance relations for the lower dimensional invariant tori

$$\frac{dH_0}{dJ_i} \Big|_{p_f^*} = 0 \Leftrightarrow \frac{d\phi_i}{dt} \Big|_{p_f^*} = 0, \quad i \in \{1, \dots, n-1\}, \quad (22)$$

where  $p_f^*$  is also a fixed point in the normal plane, namely a solution of Eq. (18) [the equivalence (22) can be easily verified by using the chain rule (18) and the fact that  $(J, \phi)$  are conjugate canonical variables<sup>33,35</sup>]. In particular, a fold of the singularity surface  $H_0(\bar{q}_f, \bar{p}_f, J_f)$  at the nonparabolic torus  $(\bar{q}_f, \bar{p}_f, J_f)$  implies that this  $n-1$ -dimensional torus is  $n-1$  resonant, namely it is a torus of fixed points. The normal stability of this torus may be elliptic or hyperbolic. Notice that the appearance of such folds is a persistent phenomenon; hence, so is the appearance of circles of fixed points in 2-d.o.f. systems (see the corresponding theorems in Ref. 17). To find a set of bifurcating energies we need to list the extremum of the surfaces  $H_0(\bar{q}_f, \bar{p}_f, J_f)$  for the various singularity manifolds. To establish that at these values the topology of the energy surface changes we also need to verify that these are nondegenerate. In Table III we list the  $I$  values for which folds are created for the six singular surfaces of Table III, all of which are indeed nondegenerate (in fact quadratic). The values of  $I$  for which the singular circles are parabolic are listed as well.

Using the resonant  $I$  values of Table III in Table IV, we conclude that the following energy values correspond to bifurcations due to the resonances/folds:

$$\begin{aligned} h_r^{pw} &= -\frac{\Omega^4}{2}, \\ h_r^{sm} &= -\frac{1}{3}(\Omega^2 + k^2)^2, \\ h_r^{pwm} &= -\frac{7}{30}(\Omega^2 + \frac{4}{7}k^2)^2 + \frac{1}{7}k^4, \quad \text{for } k < \sqrt{2}\Omega, \\ h_r^{smm} &= -\frac{\Omega^4}{2} - k^4, \quad \text{for } k < \frac{1}{\sqrt{2}}\Omega. \end{aligned} \quad (23)$$

At each of these energies the corresponding family of circles (for example  $p_{pw}$ ) has a circle of fixed points (e.g., the open triangle in diagram 3\* in Fig. 2 corresponds to a normally hyperbolic circle of fixed points, giving rise to hyperbolic

resonance under perturbations); for energies below the bifurcating energy (say for  $h < h_r^{pw}$ ; see diagrams 1 and 2 there) the energy surfaces do not include any circle of this family, whereas for energies beyond this value (say, for  $h > h_r^{pw}$ , diagram 4-10 there) two circles of this family appear on the same energy surface.

The perturbed dynamics near such circles of fixed points, occurring on these bifurcating energy surfaces, is different than the standard perturbed motion which was described in Sec. V. When the resonant circles are normally elliptic (for  $\Omega < \Omega_{pr-pw}$  for the plane-wave circles, for  $\Omega < \Omega_{pr-sm}$  for the mixed-mode circles, and for  $\Omega > \Omega_{pr-pw}$  for the plane-wave mixed circles), the coupling creates a resonance zone. Then, one expects that an even number of fixed points will survive the perturbation, half of them becoming stable and half unstable. Consider the motion near a stable point  $p_{pw}(\gamma(0))$  belonging to  $p_{pw}$  which survives the perturbation. Then,  $\gamma(T) = \gamma(0) + \tilde{\gamma}(T)$ , where  $|\tilde{\gamma}(T)|$  is small and similarly all the other components of  $p^e(T)$  remain close to  $p_{pw}(\gamma(0))$ . Hence, the corresponding  $B$ -plane plots shown in Fig. 5 are quite different—instead of seeing circles, independently of the initial phases, as in the nonresonant case, we will see asymmetric spots for some phases and circles for others.

The motion near hyperbolic resonant circles is of a completely different nature.<sup>11-14</sup> Of particular interest for the NLS model are the hyperbolic resonance plane-wave circles which exist when  $I_p^{pw} = \frac{1}{2}k^2 < I_r^{pw} = \Omega^2$ . When  $\Omega = 1$  these appear only for small wave numbers ( $k < \sqrt{2}$ ), namely for sufficiently large intervals. By introducing the additional parameter  $\Omega$ , we see that for any  $k$  value there is an interval of  $\Omega$  values for which the resonant plane-wave circle is hyperbolic: it is hyperbolic for all  $\Omega > \Omega_{pr-pw} = (1/\sqrt{2})k$ , and by Remark 1 the two-mode model is relevant for  $\Omega < \sqrt{2}k$  (indeed, the symmetric mode resonant circles are hyperbolic for  $\Omega > \Omega_{pr-sm} = \sqrt{2}k$ , so their relevance is unclear). Here, we show some perturbed trajectories which appear in the hyperbolic resonance regime. We see that the main difference between the regular homoclinic chaos and the hyperbolic resonant chaotic motion has to do with the nonuniformity in the angle variable—thus, it is not observable in the amplitude plot but is clearly seen in the  $B$ -plane plots, and the real  $B$  plot. Indeed, in Fig. 7 we show the behavior near regular homoclinic orbits, whereas Fig. 6 shows the behavior near resonant homoclinic orbits. We note that in these plots typical chaotic orbits are shown—these orbits shadow some of the countable infinity of multipulse homoclinic and heteroclinic orbits that exist due to the transverse separatrix crossings (see Ref. 1 and references therein).

### B. Branching surfaces and parabolic circles

Another source for bifurcations in the energy surface structure appears when the singularity surface has a cusp (or split in the symmetric case). For the 2-degree-of-freedom case such a cusp/splitting is associated with the appearance of a parabolic circle (for the  $n$ -d.o.f. case we look for a fold in the surface of parabolic tori, namely we look for an  $n-2$  resonant parabolic  $n-1$  tori; see Ref. 33 for precise state-

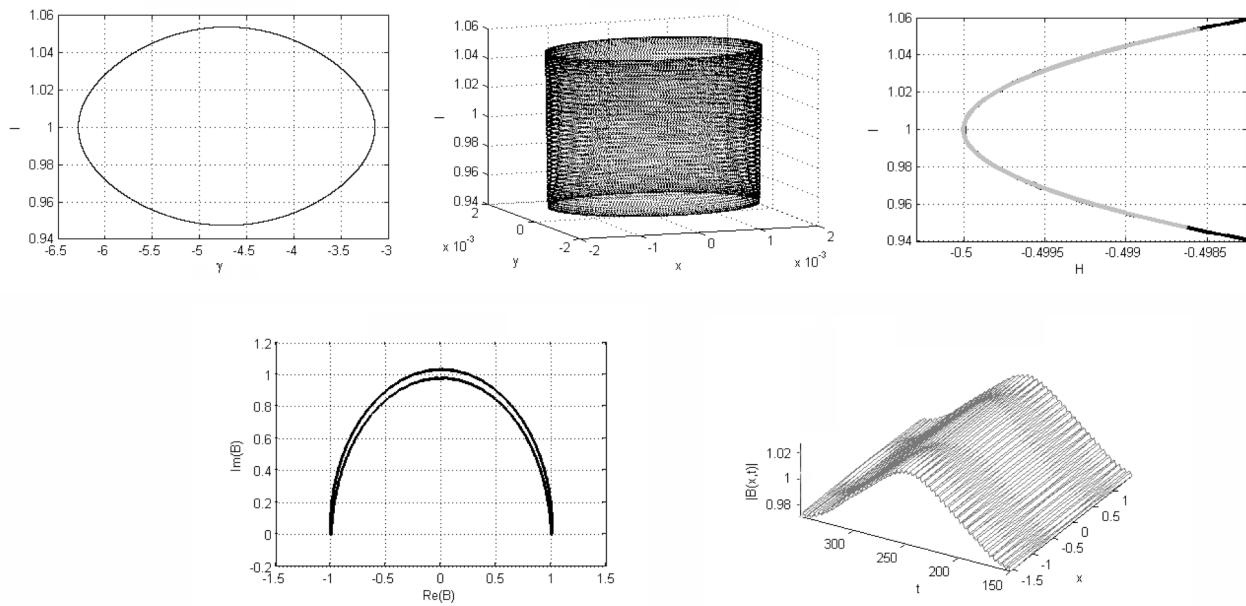


FIG. 5. A perturbed orbit near an elliptic resonant circle for  $k=2$ ,  $\epsilon=(1/\sqrt{2})10^{-3}$ . Initial conditions:  $(c(0), b(0))=(-1.413+0.001i, 0.001-0.001i)$ , i.e.,  $(x(0), y(0), I(0), \gamma(0))=(-0.001, 0.001, 0.9983, -\pi)$ .

ment). Thus, the appearance of the parabolic circle  $p_{sm}$  at  $h = h_p^{sm}$  (similarly,  $p_{pw}$  at  $h = h_p^{pw}$ ) from which the branches of circles  $p_{smm}^\pm$  emerge implies that for energies below this value (graph 1 in Fig. 2) no such circles appear, and the Fomenko graph has no splitting to two edges, whereas larger energies have these two circles as the upper boundary of the energy surface (diagrams 2–10). In Table III we list the two parabolic values of  $I$ . Plugging these values into Table IV, we find two additional values of energy bifurcations which appear due to singularity surface branchings

$$h_p^{pw} = \frac{1}{2}k^2\left(\frac{1}{4}k^2 - \Omega^2\right), \quad h_p^{sm} = k^4 - 2k^2\Omega^2. \quad (24)$$

Notice that by Remark 1 the first parabolic circle, at  $(x, y, I) = (0, 0, I_p^{pw})$ , is always in the range at which the two-mode model is expected to be valid. The second parabolic circle, at  $(u, v, I) = (0, 0, I_p^{sm})$ , occurs at an  $I$  value for which a second mode becomes unstable near the circle  $x=y=0$ . Thus, its relevance to the PDE is doubtful.

The behavior near a branching point is not simple—to analyze it one needs to understand how Hamiltonian trajectories cross bifurcations.<sup>36</sup> It appears that the action in the normal plane is a key ingredient in understanding the perturbed motion as it is adiabatically preserved.<sup>42</sup> It follows

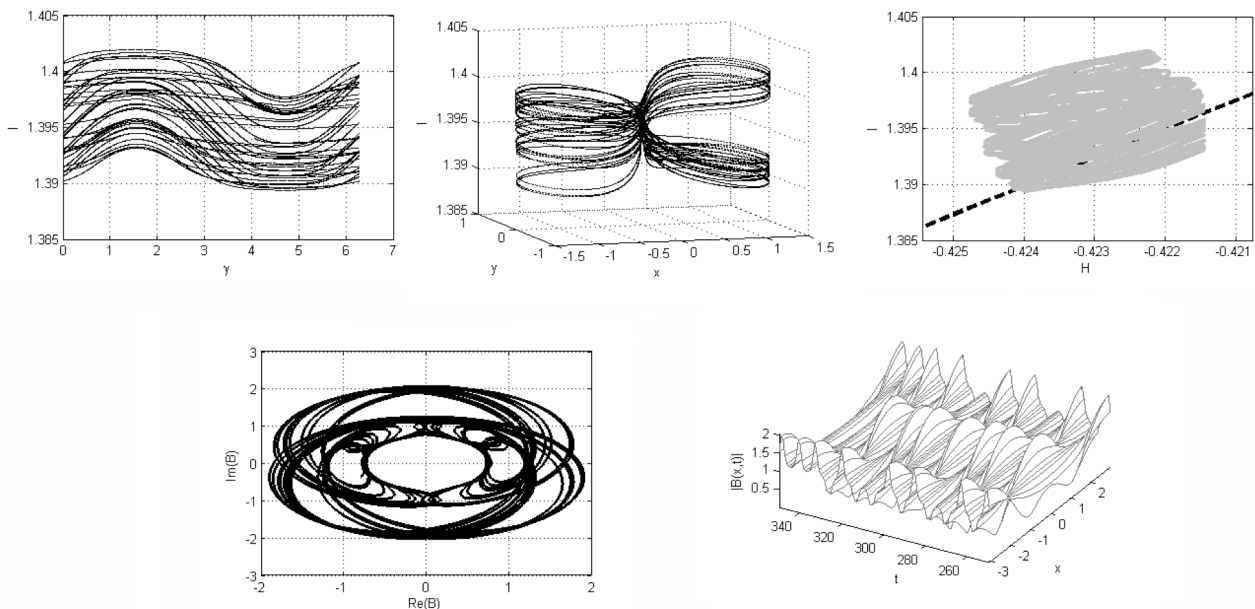


FIG. 6. A perturbed orbit near a hyperbolic resonant circle for  $k=1.025$ ,  $\epsilon=1/\sqrt{2}10^{-3}$ . Initial conditions:  $(c(0), b(0))=(-0.999-0.001i, -1.001+0.001i)$ , i.e.,  $(x(0), y(0), I(0), \gamma(0))=(1.001, -0.001, 0.9983, -\pi)$ .

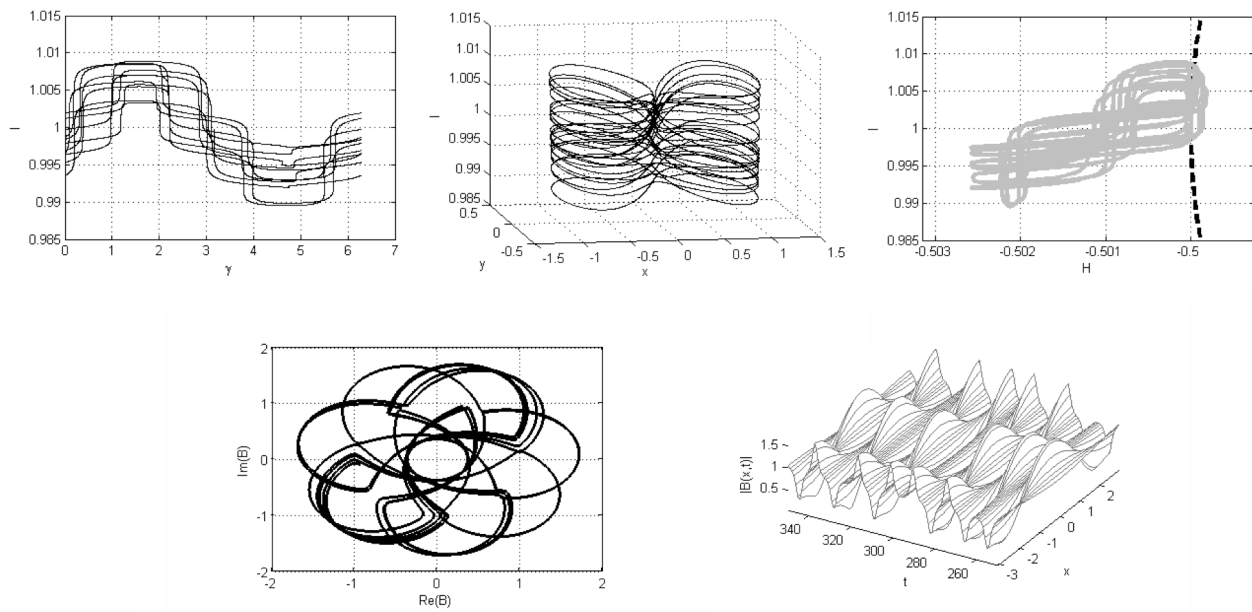


FIG. 7. A perturbed orbit near a family of hyperbolic circles for  $k=1.025$ ,  $\epsilon = \frac{1}{\sqrt{2}}10^{-3}$ . Initial conditions:  $(c(0), b(0)) = (-1.4132 - 0.001i, -0.8954 + 0.001i)$ , i.e.,  $(x(0), y(0), I(0), \gamma(0)) = (0.8954, -0.001, 1.3995, \pi)$ .

that to distinguish between the motion near a regular elliptic circle and a parabolic circle one needs to investigate very small actions in the normal plane [of the order of the action of the unperturbed homoclinic loop at energies of order  $h_p + O(\epsilon)$ ]. Only for such trajectories may the chaotic transfer across the homoclinic loop (with a chaotic zone which is exponentially small in the distance from the parabolic circle) be observed. We do not attempt to present here numerical verification for this delicate phenomenon.

**C. Singular surfaces crossings and global bifurcation**

A third possible source for topological changes in the energy surface is the crossing of singular surfaces. Such an intersection of singular surfaces of  $n-1$ -dimensional invariant tori can be a result of one of the following phenomena:

- (1) Appearance of a higher dimensional singularity, namely an  $n-2$  invariant torus.
- (2) Appearance of a global bifurcation—e.g., the creation of heteroclinic connection between two families of  $n-1$  normally hyperbolic families.
- (3) Appearance of two unrelated singular level sets for the same action and energy values. (Unrelated means that the Fomenko graphs before and after the crossings have the property that there are no edges connecting the vertices associated with these two singular surfaces.)

Each one of these phenomena appears to be persistent under  $C^r$  integrable perturbation with  $r > 2$ . The first and second cases imply that at the corresponding energy and action values there are singular orbits of a new type, whereas the third case does not. The response of the system to perturbations is therefore altered in the first and second case but not in the third. We thus call the first two dynamically significant energy bifurcation values, whereas the third is a dy-

namically insignificant energy bifurcation value. For our example, it follows from Table III that the two curves  $(H(p_{pw}(I)), I)$  and  $(H(p_{sm}(I)), I)$  cross at  $I=0$  and at  $I=I_{gb} = 4k^2$  and that no other singularity curves cross.

$I=0$  corresponds to the trivial solution  $c=b=0$ , at which both singularity curves are normally elliptic and at their intersection we have a  $4d$  elliptic point—an  $n-2$  singular level set, as in the first case above. Thus, the corresponding energy,  $h_0=0$ , is a dynamically significant energy bifurcation value.

$I_{gb}=4k^2$  corresponds to the intersection of the two singularity curves (of  $p_{pw}$  and  $p_{sm}$ ) at a value for which both families are normally hyperbolic (since  $I_{gb} > I_p^{sm} = 2k^2 > I_p^{pw} = \frac{1}{2}k^2$  for all  $k > 0$ ; see Table II). Indeed, at this value our system admits four heteroclinic connections between the plane-wave circles and the symmetric mode circles (see Ref. 14). The energy-momentum bifurcation diagrams (see Fig. 1) show the intersection between the corresponding singularity curves (dashed gray and dashed black). The Fomenko graphs (graphs 8–10 in Fig. 2) demonstrate that a global bifurcation must occur—the solid circles (that denote  $p_{sm}^\pm$ ) are connected to the open circle (that denotes  $p_{sm}$  and its homoclinic orbits) in graph 8 and to the open triangle (that denotes  $p_{pw}$  and its homoclinic orbits) in graph 10. Hence, this intersection corresponds to a global bifurcation and the corresponding energy is an energy bifurcation value. Summarizing, we find two additional energy bifurcation values resulting from the singularity surfaces crossings

$$h_0 = 0, \quad h_{gb} = 4k^2(2k^2 - \Omega^2), \tag{25}$$

and both of them are dynamically significant.

While the appearance of the global bifurcation intersection is intriguing from the mathematical point of view, it appears at values of  $I$  for which more than one unstable mode exists and the two-mode model cannot capture the full

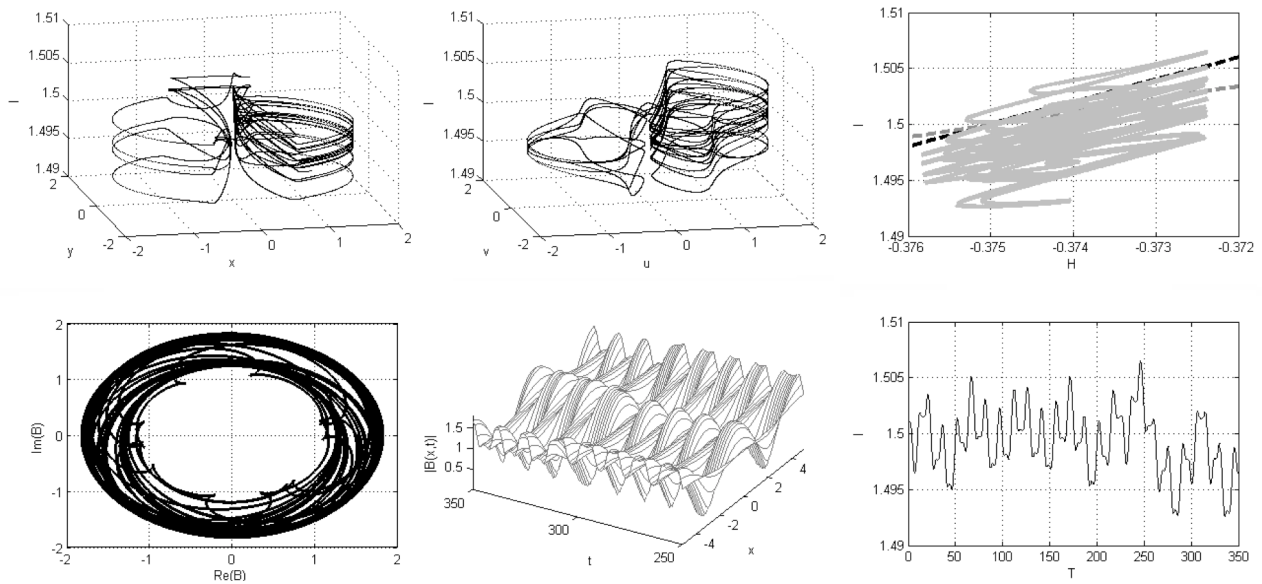


FIG. 8. A perturbed orbit near the global bifurcation for  $k=\sqrt{3}/8$ ,  $\varepsilon=(1/\sqrt{2})10^{-3}$ . Initial conditions:  $(c(0), b(0))=(-1.7311-0.001i, -0.001+0.001i)$ , i.e.,  $(x(0), y(0), I(0), \gamma(0))=(0.001, -0.001, 1.4983, \pi)$ .

dynamics (see Remark 1). Notice that the four heteroclinic connections give rise to homoclinic chains; hence, under perturbation, one expects to obtain the usual chaotic behavior associated with homoclinic chaos. Since the heteroclinic connections connect the two charts  $(x, y, I, \gamma)$  and  $(u, v, I, \theta)$ , we present in Fig. 8 the behavior in both of them, where the motion near the singular circles in each chart needs to be ignored. In Fig. 8 we present the additional  $(I, t)$  graph which is defined globally, unlike the  $(I, \gamma)$  and  $(I, \theta)$  presentations that become singular near  $c=0$  and  $b=0$ , respectively.

**D. Unbounded singularity surfaces**

We remark that another possible source for an energy bifurcation value is the appearance of a critical energy at which one of the singularity surfaces tends to infinity [i.e.,  $(H_0(p_f), J_1, \dots, J_{n-1}) \rightarrow (h_c, J_1^c, \dots, J_{j-1}^c, \infty, J_{j+1}^c, \dots, J_{n-1}^c)$ , with possibly more than one infinite direction; see Ref. 19, where it was shown that a motion in a central field may exhibit such a property]. In this case energy surfaces become unbounded in the  $J_j$  direction after this critical energy value. This possibility does not appear in our model and its dynamical implications will be studied elsewhere.

**VII. PARAMETRIC BIFURCATIONS**

The third level of the bifurcation hierarchy consists of the study of the dependence of the EMBDs on the parameters of the problem, the wave number  $k$ , and the forcing frequency  $\Omega$ . Equations (23)–(25) include the eight energy bifurcation values for our model. At these values of energies the energy surface structure changes. Hence, any singularity in the dependence of the surfaces of bifurcation values on the parameters changes the sequence of the Fomenko graphs. Fixing one of the parameters, the curves of energy bifurcation values can have singularities of the fold, asymptote, cusp, and crossing types. In our case we find that only the

latter two appear. Figure 9 shows the graph of the eight curves  $h_r^{pw}, h_p^{pw}, h_r^{sm}, h_p^{sm}, h_r^{pwm}, h_p^{pwm}, h_{gb}, h_0$  as a function of  $\Omega$  for  $k=1.025$ , and a similar figure can be constructed for these curves as a function of  $k$  for a fixed  $\Omega$  value (in principle we could expect to have some codimension two singularities but this does not appear to be the case here). This is a bifurcation diagram of the energy bifurcation values—crossings and cusps of curves in this diagram correspond to bifurcations of the EMBDs. Even for a fixed  $k$  the emerging picture is complicated—there are many intersections of these curves, so a complete description of the truncated NLS model consists of many different EMBD figures and their corresponding Fomenko graph sequences. A few representative ones are shown in Appendix B.

As in the case of crossings of singular surfaces, we observe that some of the crossings do not have dynamical significance while others do—intersections of singular surfaces which correspond to the same action values may lead to dynamical significant bifurcations. In such a case some of the orbit’s structure may be of higher codimension. Then, even for small perturbation its existence may alter the local behavior of some trajectories. These cases are enlarged in Fig. 9. Let us discuss the structure near several such external bifurcations—bifurcations of the energy bifurcation values.

**A. Parabolic resonances**

When the curve corresponding to a fold of a singular surface (indicating the existence of a torus of fixed points) and the curve corresponding to the parabolic circles intersect, a parabolic circle of fixed points is created. Indeed, at the critical value  $k=k_{pr-pw}=\sqrt{2}\Omega$  [respectively, at  $k=k_{pr-sm}=(1/\sqrt{2})\Omega$ ] the plane-wave family,  $b=0$  (respectively, the symmetric mode family,  $c=0$ ) possesses a parabolic resonant circle at  $I_{pr}=\Omega^2$ ; at this value of the parameter three bifurcating energy curves intersect:  $h_r^{pw}=h_p^{pw}=h_r^{pwm}$  (similarly, at

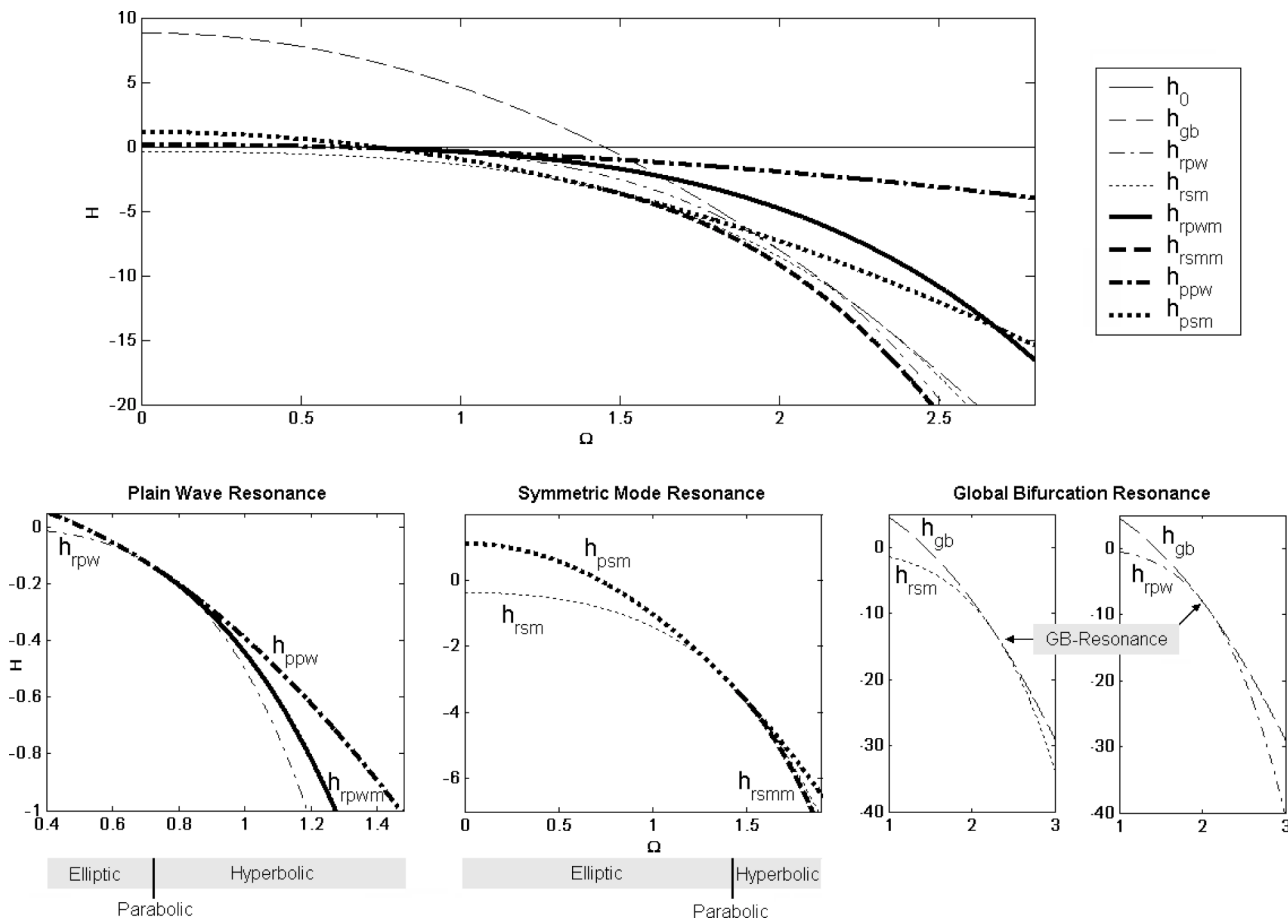


FIG. 9. Bifurcation diagram of the energy bifurcation values for  $k=1.025$ ,  $\Omega$  is varied.

$k=k_{pr-sm}$ ,  $h_r^{sm}=h_p^{sm}=h_r^{smm}$ ; see Fig. 9. The corresponding EMBD has therefore a fold occurring exactly at the point at which the singularity curve changes from solid to a dashed line.

The appearance of parabolic resonances gives rise to trajectories which have different characteristics than trajectories appearing in 1.5-d.o.f. systems and of trajectories passing through separatrices, compare Figs. 5, 7, and 10. Furthermore, it is observed (see Ref. 35) that large instabilities occur near parabolic resonances when additional degeneracies occur—when the curvature of one of the branches at the parabolic resonant points approaches zero and a near-flat PR appears (see Refs. 17 and 32 for the higher dimensional formulation and examples)

$$\left. \frac{d^2}{dJ^2} H_0(x(J), y(J), J) \right|_{p_f \rightarrow p_f^{pr}} \rightarrow 0.$$

Here, we find that  $(d^2/dI^2)H_0(x(I), y(I), I)|_{\{p_{pw}^{\pm}, p_{sm}^{\pm}, p_{pwmm}^{\pm}, p_{smm}^{\pm}\}} = \{1, \frac{3}{2}, \frac{15}{7}, 1\}$ , namely, these are fixed nonvanishing numbers. Hence, we conclude that the instability mechanism associated with the near-flat resonance does not exist in this model. It follows that an introduction of an additional parameter which controls, for example, the mixed terms in the Hamiltonian  $H_0(x, y, I)$  can alter this property and induce strong instabilities.

In Fig. 10 the perturbed motion near the plane-wave circle ( $b=0$ ) under parabolic resonance conditions ( $k = \sqrt{2}, \Omega=1$ ) is shown. Similar behavior is observed near the circle  $c=0$  in the  $(u, v, I, \theta)$  coordinates at  $k=1/\sqrt{2}, \Omega=1$  when the perturbation is of the form  $H_2(c, c^*, b, b^*) = -(i/\sqrt{2})(c-c^*) - (i\Gamma_1/\sqrt{2})(b-b^*)$ , so it does not vanish on  $c=0$ . The projections of the trajectory on the energy-momentum bifurcation diagram demonstrate that the singularity surfaces dominate the perturbed motion. The appearance of these trajectories in the  $B$ -plane plot and in the amplitude plots demonstrates that their character is different than the orbits appearing in the homoclinic and hyperbolic resonant chaotic orbits.

### B. Resonant global bifurcation

When the global bifurcation curve and the curve corresponding to a fold (circle of fixed points) intersect, a heteroclinic connection between an invariant hyperbolic circle of fixed points and an invariant hyperbolic circle is created. Such intersections occur when  $h_{gb}=h_r^{pw}$  and when  $h_{gb}=h_r^{sm}$ . Simple calculation shows that these scenarios occur at  $k = \Omega/2$  and  $k = \Omega/\sqrt{5}$ , respectively

$$I_r^{pw} = \Omega^2 = I_{gb} = 4k^2 \Leftrightarrow k = \frac{\Omega}{2},$$

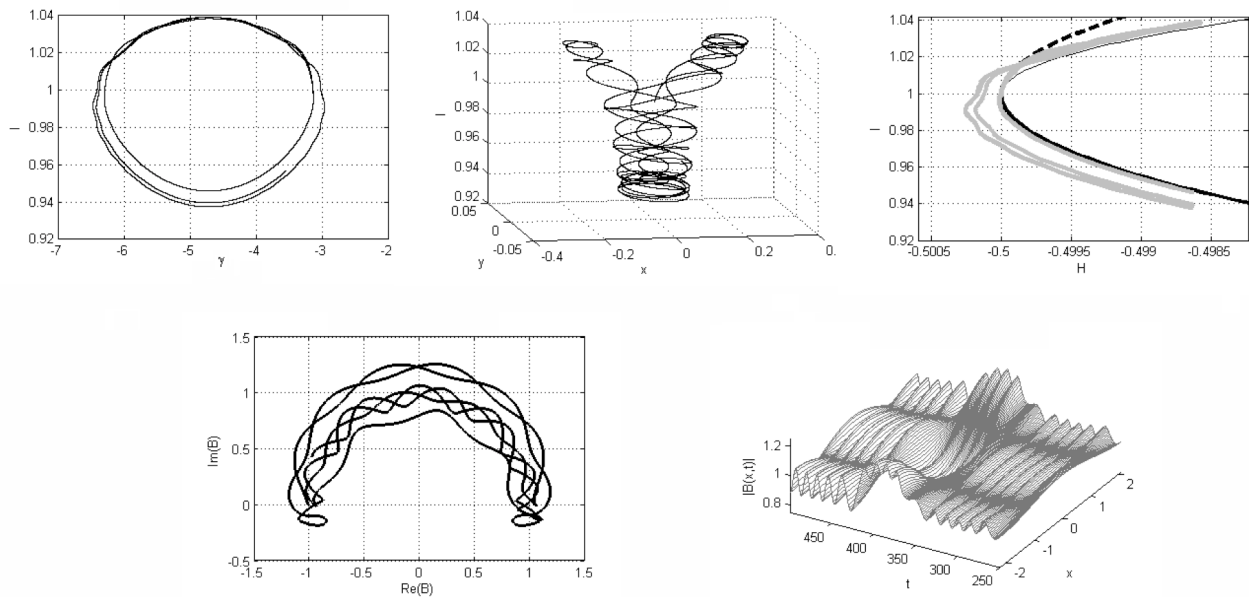


FIG. 10. A perturbed orbit near the plane-wave parabolic resonant circle for  $k=\sqrt{2}$ ,  $\varepsilon=(1/\sqrt{2})10^{-3}$ . Initial conditions:  $(c(0),b(0))=(-1.4132-0.001i, -0.001+0.001i)$ , i.e.  $(x(0),y(0),I(0),\gamma(0))=(0.001,-0.001,0.9986,-\pi)$ .

$$I_r^{sm} = \frac{2(\Omega^2 + k^2)}{3} = I_{gb} = 4k^2 \Leftrightarrow k = \frac{\Omega}{\sqrt{5}} = 0.4472\Omega.$$

In fact, as is seen from Fig. 9, and may be easily verified at  $k=\Omega/2$  (respectively, at  $k=\Omega/\sqrt{5}$ ), the curves  $h_{gb}$  and  $h_r^{pw}$  (respectively,  $h_r^{sm}$ ) are tangent. It implies that for  $k$  values in the range  $(0.4472\Omega, 0.5\Omega)$  near-resonant behavior of both circles involved in the global bifurcations is expected if  $\varepsilon$  is not very small (generally, we expect that with two parameters a global bifurcation between two resonant circles may be found—but this is not the case here).

Geometrically, at these values of  $k$  the unperturbed system has a circle of fixed points [at  $p_{pw}(I_{rgb-pw})$  and  $p_{sm}(I_{rgb-sm})$ , respectively; see Table III] which has four families of heteroclinic connections to a periodic orbit [at  $p_{sm}(I_{rgb-pw})$  and  $p_{pw}(I_{rgb-sm})$ , respectively]. The behavior of such a structure under small perturbations has not been analyzed yet, to the best of our knowledge. Simulations near these two values reveal an intriguing picture of instability which is not well understood yet. In Fig. 11, a representative simulation is presented. We note again that the relevance of such trajectories to the PDE model is questionable (remark 1), yet the general phenomenon of a family of heteroclinic connections between a circle of fixed points and a periodic orbit is robust as a codimension one phenomenon in 2-d.o.f. systems (and hence is expected to be a persistent phenomenon in  $n$ -d.o.f. systems with  $n > 2$ ).

### C. Other crossings

Notice that several other crossings exist—these do imply topological changes on the sequences of the Fomenko graphs but do not imply that the local qualitative behavior of solutions will be altered. For example, the global bifurcation energy and the parabolic bifurcation energy of the two corre-

sponding circles cross when  $h_{gb}=h_p^{pw}$  and when  $h_{gb}=h_p^{sm}$ . However, it is immediately seen that the  $I$  values at which the global bifurcations occurs ( $I_{gb}=4k^2$ ) and the  $I$  values at which parabolicity appears ( $I_p^{pw}=\frac{1}{2}k^2, I_p^{sm}=2k^2$ ) are well separated for all  $k$  values which are bounded away from 0. Hence, the dynamics associated with these two phenomena appears on separate phase-space regions and the coincidence of these two energy bifurcation values is not dynamically significant.

Finally, at  $k=0$  many of the curves cross; thus, in the limit of small  $k$  we expect quite a complicated behavior as many of the bifurcations occur for very nearby  $I$  values and the curvature of all the curves in the EMBD are quite small. As we have mentioned—small curvature means degeneracies and strongest possible instabilities. However, by Remark 1, all these phenomena are relevant only for small  $I$  (quadratic in  $k$ ) values.

## VIII. CONCLUSIONS

Two main themes were developed in parallel in this paper—on one hand global analysis of a specific model—the truncated forced NLS system was studied, and on the other a general framework for analyzing such near-integrable systems was suggested. Let us first summarize the main features of this framework and then relate to the specific results regarding the truncated forced NLS.

Given an integrable family of Hamiltonian systems  $H_0(\bar{q}, \bar{p}, J; \mu)$  depending on the vector of parameters  $\mu$ , we propose that the following three-level hierarchy of bifurcation scenario organizes all possible behaviors under small perturbations:

- The first level consists of the values of the constants of motion across which the topology of the level sets on a

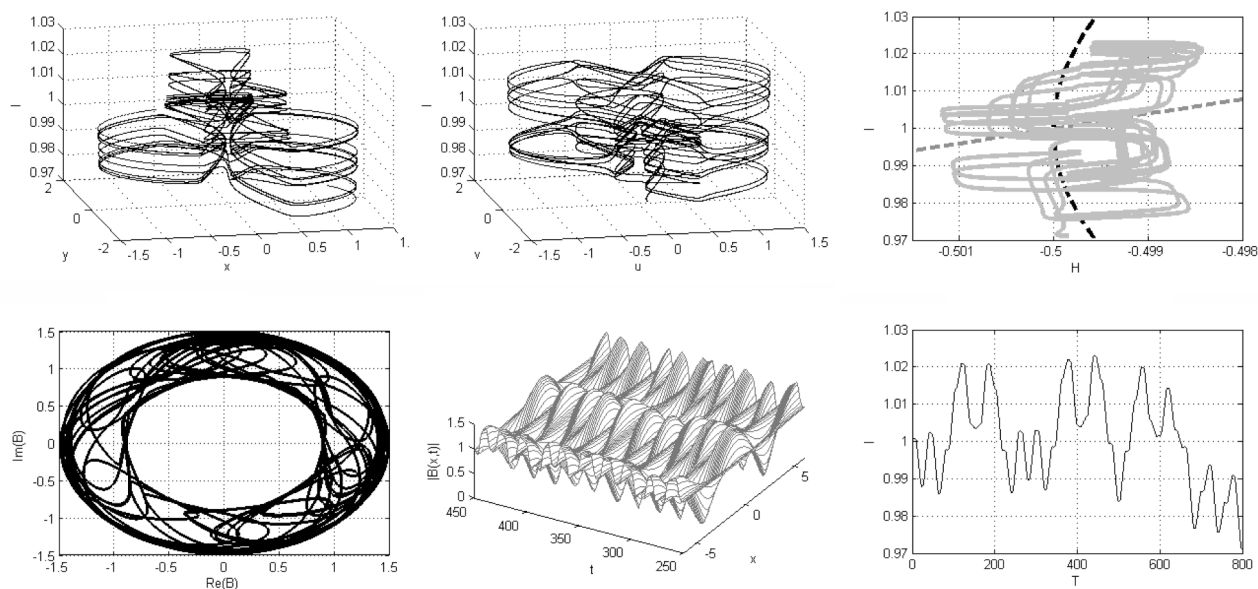


FIG. 11. A perturbed orbit near a resonant global bifurcation for  $k=1/2, \epsilon=(1/\sqrt{2}), 10^{-3}$ . Initial conditions:  $(c(0), b(0))=(-1.4132-0.001i, -0.001+0.001i)$ , i.e.  $(x(0), y(0), I(0), \gamma(0))=(0.001, -0.001, 0.9986, -\pi)$ .

given energy surface  $H_0(\bar{q}, \bar{p}, J; \mu)=h$  is changed. These are the values at which the singularity surfaces cross the vertical hyperplane  $H_0=h$  on the energy momentum bifurcation diagrams, and correspond to the vertices in the Fomenko graphs.

- The second level consists of the energy bifurcation values  $h^b$  at which the form of the Fomenko graph changes, namely across which the energy surfaces are no longer  $C^1$  conjugate by a near-identity mapping. Thus, it describes how the energy surface differential topology is changed with  $h$ .
- The third level consists of the bifurcating parameter values  $\mu^b$  at which the bifurcation sequence of the second level changes.

Most previous works have concentrated on the first level alone, by which the topology of level sets on a given energy surface are studied. For a large class of systems the Fomenko graphs (and the corresponding branched surfaces in higher dimensions) provide a full description of this level. The second and third level of this hierarchy have not been explicitly identified and described. Though Ref. 31 discusses the second level, it is mainly done with respect to the appearance of fixed points in 2-degrees-of-freedom systems. The bifurcations of the second level are the energy values at which the singular surfaces of the first level are singular with respect to projections on the energy axis. For  $n=2$  we have described four types of such singularities: folds, cusps, crossings, and asymptotes. We have shown that these singularities may be associated with certain dynamical phenomena:

- (1) Folds are associated with  $n-1$ -dimensional resonant tori.
- (2) Cusps are associated with  $n-1$ -dimensional parabolic tori.
- (3) Crossings of two surfaces are associated with either  $n$

$-2$ -dimensional tori, global bifurcations, or unrelated dynamical phenomena which occur simultaneously (this list may be nonexhaustive).

- (4) The asymptotes to infinity were not investigated in this context yet.

The third level, at which the singularities of the projection of the energy bifurcation surfaces onto the parameter space are found, reveals the existence of locally degenerate solutions. In particular, we have shown that the parabolic resonance phenomena and the resonant global bifurcation phenomena are associated with such singularities, and that these appear in the truncated NLS model.

Indeed, applying these tools to analyze the truncated forced NLS equations led to several new insights. First, we were led by the analysis to introduce a second parameter, the frequency of the forcing  $\Omega$  and showed that for *any given wave number*  $k$  hyperbolic resonance appears for an open interval of  $\Omega$  values, whereas parabolic resonance appears at isolated  $\Omega$  values. For any  $k$ , both types of resonances appear with amplitudes for which the two-mode model is expected to be valid; thus, by tuning the forcing frequency inherently different dynamics may be produced. Second, we observe that each of the bifurcations listed in the hierarchical structure produces, in the near-integrable system, a different type of perturbed orbit in an open neighborhood of the bifurcation values. In particular, we demonstrate that orbits associated with elliptic resonances, homoclinic chaos, hyperbolic resonances, parabolic resonances, global bifurcations, and resonant global bifurcations have different characteristics in various projections. Presently, we seek tools for making a more precise distinction between these various types of trajectories.

The relation between the new Hamiltonian finite-dimensional results (the appearance of parabolic resonances

and resonant global bifurcations in this model) and the PDE solutions is under current investigation. One would hope that these will turn out to produce finite-dimensional dissipative analogs and infinite-dimensional conservative and dissipative analogs as did the hyperbolic resonance scenario.

**ACKNOWLEDGMENTS**

This research was supported by the Israel Science Foundation (Grant No. 926/04) and by the Minerva Foundation.

**APPENDIX A**

**Closeness of perturbed and unperturbed energy surfaces**

Here, we prove Theorem 1: Consider a near-integrable Hamiltonian  $H(q, p; \varepsilon) = H_0(q, p) + \varepsilon H_1(q, p; \varepsilon)$ ,  $\varepsilon \ll 1$ ,  $(q, p) \in M$ , where  $M$  is a  $2n$ -dimensional symplectic manifold and  $H$  satisfies the boundness Property 1. Consider the energy surface  $M^\varepsilon(h) = \{(q^\varepsilon, p^\varepsilon) | H(q^\varepsilon, p^\varepsilon; \varepsilon) = h\}$ . Then, for each  $\delta > 0$  there exists an  $\varepsilon_0(\delta)$  and a constant  $K(\delta)$  (independent of  $h$ ) such that for all  $0 \leq \varepsilon < \varepsilon_0(\delta)$ , and for all  $(q^\varepsilon, p^\varepsilon) \in M^\varepsilon(h)$  satisfying

$$\|\nabla H_0(q^\varepsilon, p^\varepsilon)\| > \delta, \tag{A1}$$

there exists  $(q^0, p^0) \in M^0(h)$  [i.e.,  $H_0(q^0, p^0) = h$ ] such that  $\|(q^\varepsilon, p^\varepsilon) - (q^0, p^0)\| < K(\delta)\varepsilon$ .

*Proof:* Roughly, the proof is a simple application of the implicit function theorem, with a continuation argument which shows that a sufficiently small  $\varepsilon_0(\delta)$  may be chosen so that the gradient of  $H$  is bounded away from zero on the interval  $[0, \bar{\varepsilon}]$  for all  $0 \leq \bar{\varepsilon} < \varepsilon_0(\delta)$ .

First, let us prove that there exists an  $\varepsilon_2(\delta)$  such that for all  $0 \leq \bar{\varepsilon} < \varepsilon_2(\delta)$  there exists at least one coordinate, say, with no loss of generality,  $q_1$ , such that  $|\partial H / \partial q_1|_{(q^\varepsilon, p^\varepsilon)}| > \delta / (2\sqrt{2n})$ .

Choose  $L_1, \varepsilon_1$  so that Property 1 is satisfied with  $L_2 = 1$ . Let

$$K_1 = \max_{\varepsilon \in [0, \varepsilon_1]} \{ \max_{B_{2L_1}} \|\nabla H_1(q, p; \varepsilon)\| \}, \tag{A2}$$

where  $B_L = \{(q, p) | \|(q, p)\| \leq L\}$ . Consider a point (which is not a fixed point) on the perturbed energy surface  $(q^\varepsilon, p^\varepsilon) \in M^\varepsilon(h)$ , so that  $H(q^\varepsilon, p^\varepsilon; \varepsilon) = h$  and  $\|\nabla H_0(q^\varepsilon, p^\varepsilon)\| > \delta$  for some  $\delta$ . It follows that there exists at least one coordinate, say, with no loss of generality,  $q_1$ , such that  $|\partial H_0 / \partial q_1|_{(q^\varepsilon, p^\varepsilon)}| > \delta' = \delta / \sqrt{2n}$ . Hence, for  $(q^\varepsilon, p^\varepsilon) \in M^\varepsilon(h) \cap B_{L_1}$  satisfying (A1), for all  $\bar{\varepsilon} < \min\{\varepsilon_1, \delta' / 2K_1\}$  we immediately get that  $|\partial H / \partial q_1|_{(q^\varepsilon, p^\varepsilon)}| > \delta' - \bar{\varepsilon}K_1 > \frac{1}{2}\delta'$ . If  $M^\varepsilon(h)$  is large, so that there exist  $(q^\varepsilon, p^\varepsilon) \in M^\varepsilon(h)$  satisfying  $\|(q^\varepsilon, p^\varepsilon)\| > L_1$ , then by Property 1, for all  $\bar{\varepsilon} < \varepsilon_1$ ,  $\|\nabla H_1(q^\varepsilon, p^\varepsilon; \varepsilon)\| < \|\nabla H_0(q^\varepsilon, p^\varepsilon)\|$ . Assume with no loss of generality that  $|\partial H_0 / \partial q_1|_{(q^\varepsilon, p^\varepsilon)}| = \max_{i \in \{1, \dots, n\}} \times \{|\partial H_0 / \partial q_i|_{(q^\varepsilon, p^\varepsilon)}|, |\partial H_0 / \partial p_i|_{(q^\varepsilon, p^\varepsilon)}|\}$ . Then

$$\begin{aligned} \left| \frac{\partial H_1}{\partial q_1} \right|_{(q^\varepsilon, p^\varepsilon)} &\leq \|\nabla H_1(q^\varepsilon, p^\varepsilon; \varepsilon)\| \\ &< \|\nabla H_0(q^\varepsilon, p^\varepsilon)\| < \sqrt{2n} \left| \frac{\partial H_0}{\partial q_1} \right|_{(q^\varepsilon, p^\varepsilon)}, \end{aligned}$$

thus

$$\left| \frac{\partial H}{\partial q_1} \right|_{(q^\varepsilon, p^\varepsilon)} > \left| \frac{\partial H_0}{\partial q_1} \right|_{(q^\varepsilon, p^\varepsilon)} (1 - \sqrt{2n\bar{\varepsilon}}) > \frac{1}{2}\delta',$$

for  $\bar{\varepsilon} < \min\{\varepsilon_1, 1 / (2\sqrt{2n})\}$ .

Summarizing, we established that  $|\partial H / \partial q_1|_{(q^\varepsilon, p^\varepsilon)}| > \frac{1}{2}\delta' = \delta / (2\sqrt{2n})$  for all  $(q^\varepsilon, p^\varepsilon) \in M^\varepsilon(h)$  satisfying Eq. (A1) provided  $\bar{\varepsilon} < \varepsilon_2(\delta) = \min\{1 / (2\sqrt{2n}), \delta / (2\sqrt{2n}) / K_1, \varepsilon_1\}$  where  $K_1$  is defined by (A2) and  $L_1$  is the smallest constant for which Eq. (11) is satisfied with  $L_2 = 1$ .

By the implicit function theorem, since  $(q^\varepsilon, p^\varepsilon)$  solves  $H(q^\varepsilon, p^\varepsilon; \varepsilon) = h$ , and there exists one coordinate, say  $q_1$ , such that  $|\partial H_1 / \partial q_1|_{(q^\varepsilon, p^\varepsilon)}|$  is bounded away from zero, it follows that for  $\bar{\varepsilon} < \varepsilon_2(\delta)$  the equation  $H(q^\varepsilon, p^\varepsilon; \varepsilon) = h$  has a solution for  $|\varepsilon - \bar{\varepsilon}|$  small. Moreover, a unique solution of the form  $(q^\varepsilon, p^\varepsilon) = (x(\varepsilon), q_2^\varepsilon, \dots, q_n^\varepsilon, p^\varepsilon)$  where  $x(\varepsilon) = q_1(q_2^\varepsilon, \dots, q_n^\varepsilon, p^\varepsilon, \varepsilon)$  may be found by solving the initial value problem

$$\begin{aligned} \frac{dx}{d\varepsilon} &= - \frac{H_1(x, q_2^\varepsilon, \dots, q_n^\varepsilon, p^\varepsilon, \varepsilon) + \varepsilon \frac{\partial H_1(x, q_2^\varepsilon, \dots, q_n^\varepsilon, p^\varepsilon, \varepsilon)}{\partial \varepsilon}}{\frac{\partial H(x, q_2^\varepsilon, \dots, q_n^\varepsilon, p^\varepsilon, \varepsilon)}{\partial q_1}} \\ &= F(x, \varepsilon), \end{aligned} \tag{A3}$$

$$x(\bar{\varepsilon}) = q_1^\varepsilon.$$

Since  $F(x, \varepsilon)$  is smooth and bounded near  $(q_1^\varepsilon, \bar{\varepsilon})$ , a unique solution locally exists. We need to show that this solution may be extended to the interval  $[0, \bar{\varepsilon}]$ . For  $(q^\varepsilon, p^\varepsilon) \in B_{\frac{3}{2}L_1}$ ,  $H_1$  and its derivatives are bounded, and since  $|\partial H / \partial q_1|_{(q^\varepsilon, p^\varepsilon)}| > \delta / (2\sqrt{2n})$  independent of  $\bar{\varepsilon}$  (for all  $\bar{\varepsilon} < \varepsilon_2(\delta)$ ), it follows that  $|F(x, \varepsilon)|$  remains bounded on the interval  $[0, \bar{\varepsilon}]$  for sufficiently small  $\bar{\varepsilon}$ . For  $\|(q^\varepsilon, p^\varepsilon)\| > \frac{3}{2}L_1$ , rescale Eq. (A3) by  $\|(q^\varepsilon, p^\varepsilon)\|$ , then Eq. (11) and the choice of  $q_1$  as the direction at which  $\nabla H_0(q^\varepsilon, p^\varepsilon)$  is maximal, guarantees again that  $|F(x, \varepsilon)| / \|(q^\varepsilon, p^\varepsilon)\|$  remains bounded on the interval  $[0, \bar{\varepsilon}]$  for sufficiently small  $\bar{\varepsilon}$  [the choice of  $\frac{3}{2}L_1$  guarantees that for sufficiently small  $\bar{\varepsilon}$  the inequalities (11) and the bound  $K_1$  will hold for all  $x(\varepsilon)$ ]. ■

**Application to the truncated NLS model**

Since the unperturbed energy may be written in the form

$$\begin{aligned} H_0 &= \frac{1}{8}|c|^4 + \frac{3}{16}|b|^4 + \frac{1}{2}|b|^2|c|^2 \left(1 + \frac{1}{2} \cos(2 \arg(bc^*))\right) \\ &\quad - \frac{1}{2}(1+k^2)|b|^2 - \frac{1}{2}|c|^2, \end{aligned} \tag{A4}$$

namely all its quartic terms have positive coefficients, whereas the perturbation is linear in  $|c|$ ,  $|b|$ , it follows immediately that indeed for sufficiently large  $|c|$ ,  $|b|$  both the unperturbed energy and its gradient magnitude are much larger

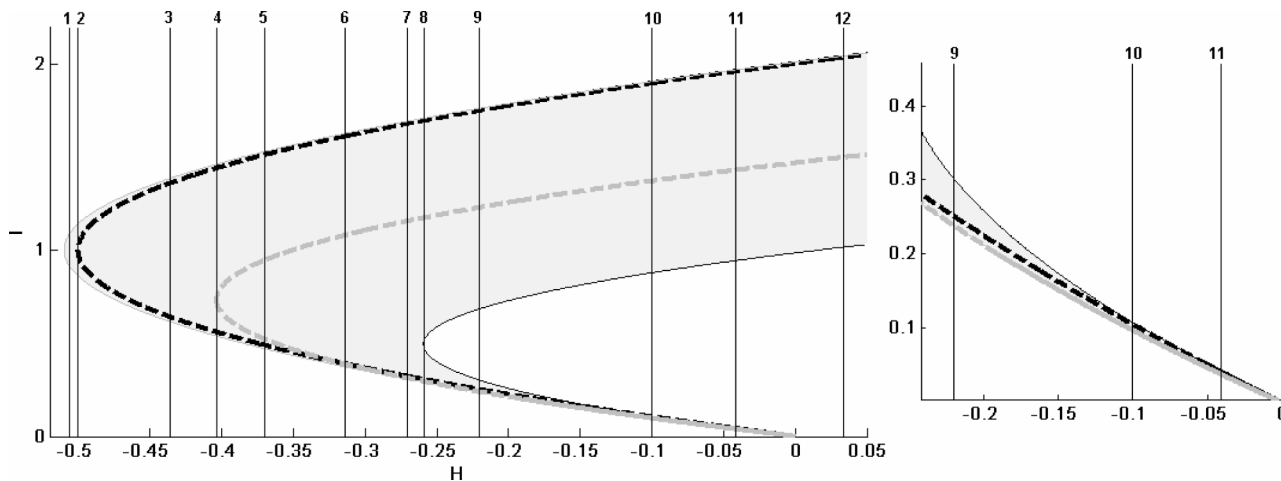


FIG. 12. EMBD graph for  $k = \sqrt{1/10}$ .

than the perturbation and its gradient as needed for the theorem to apply.

Denote by  $c_{\max}^{h,\epsilon}$ ,  $b_{\max}^{h,\epsilon}$  the maximal amplitude of  $c, b$  on the energy surface  $H(c, c^*, b, b^*; \epsilon) = h$

$$c_{\max}^{h,\epsilon} = \max\{|c| : H(c, c^*, b, b^*; \epsilon) = h\},$$

$$b_{\max}^{h,\epsilon} = \max\{|b| : H(c, c^*, b, b^*; \epsilon) = h\},$$

it follows from (A4) that for  $h \gg 1$ ,  $c_{\max}^{h,0}, b_{\max}^{h,0} = O(\sqrt[4]{h})$ . Furthermore, it can be shown, using the form of Eq. (7), that for large values of  $h$  the system cannot have fixed points. In fact, one can prove the following:

*Lemma:* There exists an  $h^*(k)$  such that if  $h > h^*(k)$ , then  $\|\nabla H_0|_{H_0(c,c^*,b,b^*)=h}\| \neq 0$ .

*Proof:* Let us find all solutions to  $\|\nabla H_0|_{H_0(c,c^*,b,b^*)=h}\| = 0$ . Clearly, at  $c=b=0$   $\|\nabla H_0|_{H_0(c,c^*,b,b^*)=h}\| = 0$ , so  $h^*(k) > 0 = H_0(0, 0, 0, 0)$ . Using the nonsingular transformation to the  $(x, y, I, \gamma)$  coordinates for  $c \neq 0$ , and the nonsingular transformation to the  $(u, v, I, \theta)$  coordinates when  $b \neq 0$ , it follows that  $\|\nabla H_0|_{H_0(c,c^*,b,b^*)=h}\| = 0$  only when the invariant circles of Table I are circles of fixed points, namely at the resonant  $I$  values,  $I = I_r$ , of Table III. Plugging these resonant  $I$  values into Table III, we find that circles of fixed points appear at the following  $h$  values:  $H_0(p_{f\text{-res}}) = \{-\frac{1}{2}, -\frac{1}{3}k^4 - \frac{2}{3}k^2 - \frac{1}{3}, \frac{1}{15}k^4 - \frac{4}{15}k^2 - \frac{7}{30}, -\frac{1}{2} - k^4\}$ . It follows that for all  $h > \frac{1}{15}k^4$  there are no fixed points on the energy surfaces. ■

In fact, it follows from (7) that for  $h$  sufficiently large, for all  $(c, b)$  satisfying  $H_0(c, c^*, b, b^*) = h$ , we have

$$\max\left\{\left|\frac{\partial H_0(c, c^*, b, b^*)}{\partial b^*}\right|, \left|\frac{\partial H_0(c, c^*, b, b^*)}{\partial c^*}\right|\right\} \geq Ch^{3/4}.$$

It follows from the implicit function theorem and the form of the perturbation [namely, since  $H_i(i=1, 2)$  are linear in  $c, b$  so that  $|H_i| < O(\sqrt[4]{h})$ ], that for  $\epsilon = o(\sqrt[4]{h})$

$$c_{\max}^{h,\epsilon} = c_{\max}^{h,0} + O\left(\frac{\epsilon}{\sqrt[4]{h}}\right),$$

$$b_{\max}^{h,\epsilon} = b_{\max}^{h,0} + O\left(\frac{\epsilon}{\sqrt[4]{h}}\right).$$

So, formally, the larger the  $h$  the larger the extent of the energy surface and the larger the range of unperturbed energy surfaces which we need to consider. However, if  $h$  is very large the structure of  $H_0$  remains asymptotically unchanged and one can verify that in fact this limit may be studied by rescaling; substituting

$$\bar{c} = \frac{c}{\sqrt[4]{h}}, \quad \bar{b} = \frac{b}{\sqrt[4]{h}},$$

leads to

$$H(c, c^*, b, b^*) = h \left( H_0(\bar{c}, \bar{c}^*, \bar{b}, \bar{b}^*) + O\left(\frac{1}{\sqrt[4]{h}}\right) + \frac{\epsilon}{h^{3/4}} H_i(\bar{c}, \bar{c}^*, \bar{b}, \bar{b}^*) \right),$$

namely to the near-integrable motion with finite  $h$ .

### APPENDIX B: DIAGRAMS' DEPENDENCE ON PARAMETERS

A few representative EMBD and Fomenko graphs are presented in Figs. 12–17 to demonstrate possible different sequences of energy bifurcation values in our model when the wave number  $k$  is varied and the forcing frequency is fixed to  $\Omega = 1$ . In Figs. 12 and 13 the sequence of eight energy bifurcation values is  $(h_r^{smm}, h_r^{pw}, h_r^{sm}, h_{gb}, h_r^{pwm}, h_p^{sm}, h_p^{pw}, h_0)$  for  $k = \sqrt{1/10}$ . Whereas, in Figs. 14 and 15 the value of  $k$  is increased to  $k = \sqrt{9/40}$  and the sequence is altered to  $(h_r^{smm}, h_r^{sm}, h_r^{pw}, h_{gb}, h_p^{sm}, h_r^{pwm}, h_p^{pw}, h_0)$ . Furthermore, in this case, the global bifurcation value ( $h_{gb}$ ) is close to the folds of the two dashed lines  $(h_r^{sm}, h_r^{pw})$  which correspond to resonances of the symmetric mode circle  $-p_{sm}$  and the plane wave circle  $-p_{pw}$ . It follows (and observed numerically) that for  $\epsilon = O(|h_{gb} - h_r^{sm}|) = O(0.05)$  trajectories near  $p_{pw}$  visit the neighborhood of the global bifurcation region and the re-

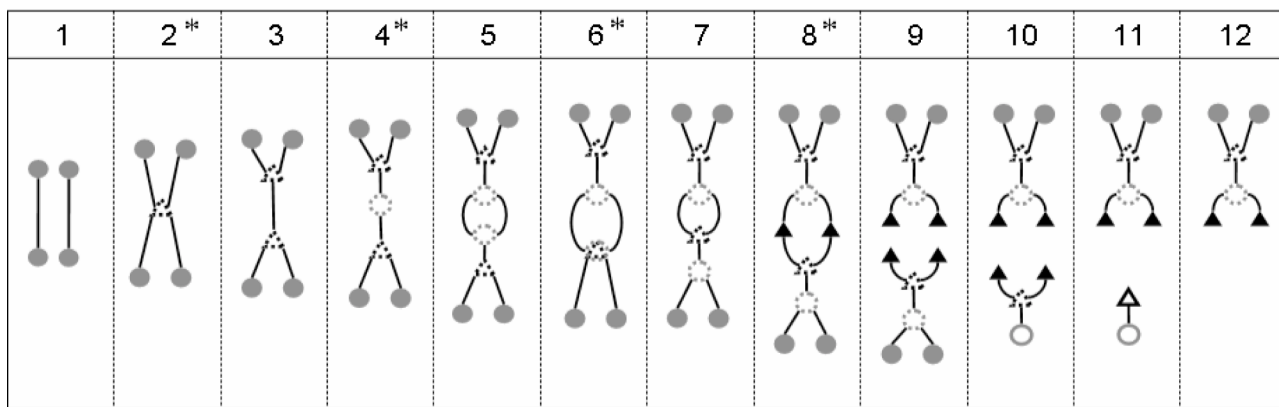


FIG. 13. Fomenko graphs figure for  $k=\sqrt{1/10}$ .

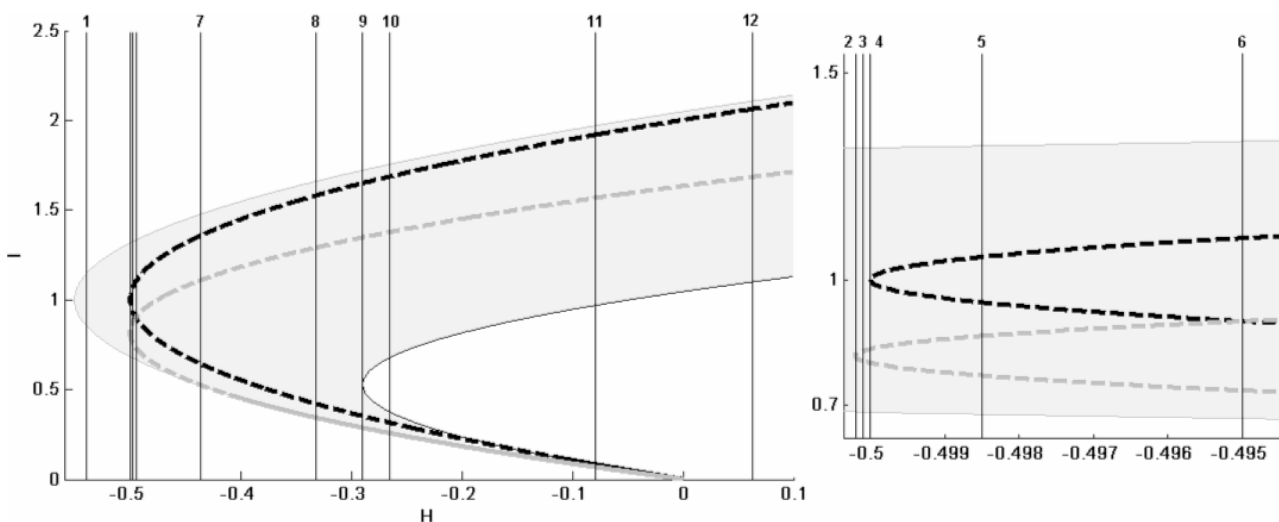


FIG. 14. EMBD graph for  $k=\sqrt{9/40}$ .

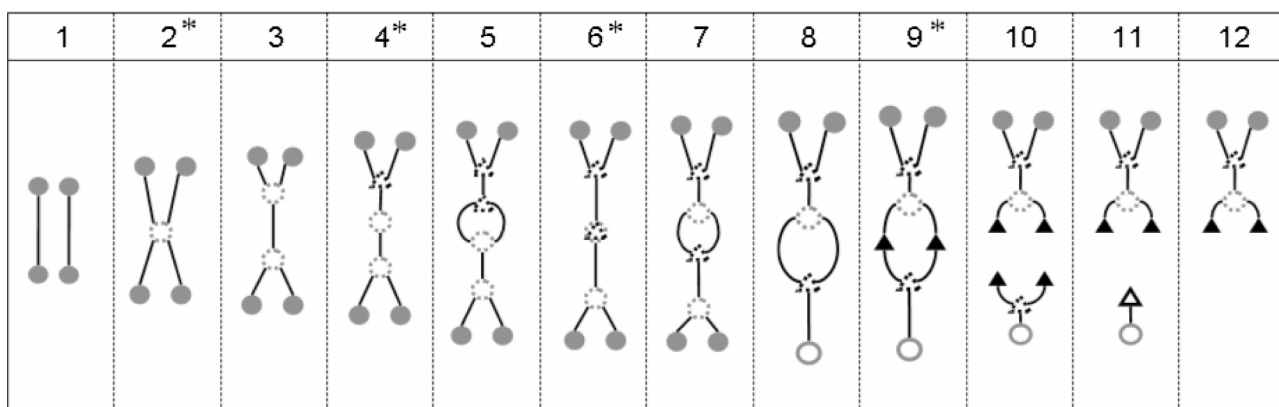


FIG. 15. Fomenko graphs figure  $k=\sqrt{9/40}$ .

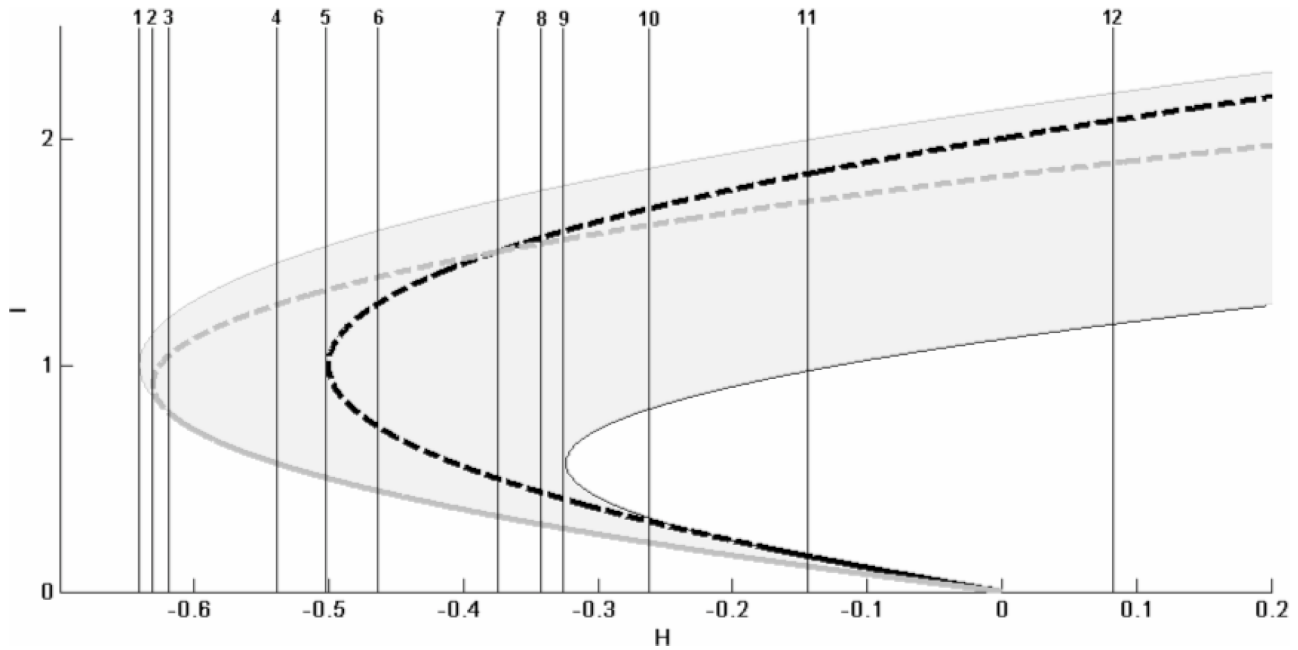


FIG. 16. EMBD graph for  $k = \sqrt{3/8}$ .

gions of hyperbolic resonances of both circles.

In Figs. 16 and 17 the value of  $k$  is further increased to  $k = \sqrt{3/8}$  and the sequence changes to  $(h_r^{smm}, h_r^{sm}, h_p^{sm}, h_r^{pw}, h_{gb}, h_r^{pwm}, h_p^{pw}, h_0)$ . Here, the parabolic point ( $h_p^{sm}$ ) is close to resonances of the symmetric mode circle ( $h_r^{sm}$ ) and the symmetric mixed mode circle ( $h_r^{smm}$ ). Numerical simulations show that perturbed orbits near these values have similar characteristics to parabolic resonance.

In the EMBD the thick (thin) black line corresponds to the plane wave family  $p_{pw}$  (the mixed mode emanating from it,  $p_{pwm}$ ). The thick (thin) gray line corresponds to the symmetric mode family  $p_{sm}$  (the mixed mode emanating from it,  $p_{smm}$ ). These curves are dashed (full) when the corresponding circle is hyperbolic (elliptic). On the Fomenko graphs, we denote the invariant circles corresponding to the plane wave family ( $p_{pw}$ ) and the invariant circles which emanate from the ( $p_{pwm}^\pm$ ), by open and full black triangles, respectively (for clarity, the boundary of the triangle is dashed when it is normally hyperbolic and full when it is normally elliptic).

The invariant circles corresponding to the symmetric mode family ( $p_{sm}$ ) and the invariant circles which emanate from them ( $p_{smm}^\pm$ ), are denoted by open and full gray circles, again with the usual convention for the stability.

**APPENDIX C: FROM SINE-GORDON TO NLS**

Bishop *et al.*<sup>3-9</sup> investigated the chaotic attractor of the damped driven sine-Gordon equation (SGE) with even spatial symmetry and periodic boundary conditions

$$u_{tt} - u_{xx} + \sin u = \delta(-\hat{\alpha}u_t + \hat{\Lambda}u_{txx} + \hat{\Gamma} \cos(\omega t)), \quad (C1)$$

$$u(x, t) = u(x + L, t), \quad u_x(0, t) = 0,$$

where  $\omega$  is the driving frequency,  $L$  is the box size,  $\delta\hat{\Gamma}$  is the driving amplitude,  $\delta\hat{\alpha}$  is the damping, and  $\delta\hat{\Lambda}$  is an additional wave-number-dependent damping term which was introduced in Ref. 14. The NLS approximation for the SGE is obtained by developing a small amplitude envelope approxi-

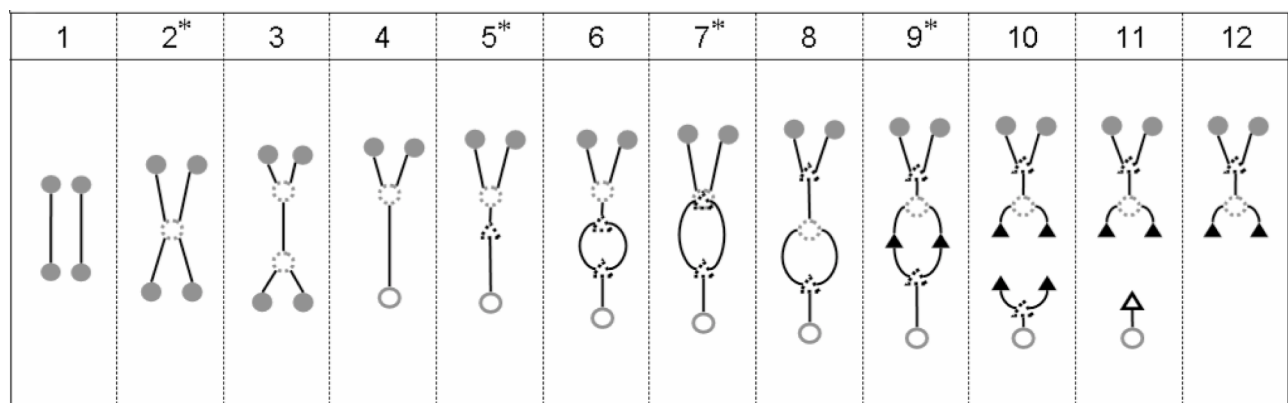


FIG. 17. Fomenko graphs figure for  $k = \sqrt{3/8}$ .

mation for the near-resonance frequency ( $\omega=1-\delta\tilde{\omega}$ ) case. More precisely, one looks for solutions of the SGE of the form

$$u = 2\sqrt{\delta\tilde{\omega}}[B_\delta(X,T)e^{i\omega t} + B_\delta(X,T) * e^{-i\omega t}], \quad (C2)$$

where  $B_\delta(X,T)$  is assumed to be analytic in  $\delta$ , and

$$\omega = 1 - \delta\tilde{\omega}, \quad X = \sqrt{2\delta\tilde{\omega}}x, \quad T = \delta\tilde{\omega}t.$$

Introducing a small parameter  $\varepsilon$  such that

$$\hat{\Lambda} = \varepsilon\Lambda, \quad \hat{\Gamma} = \varepsilon 8\delta^{3/2}\tilde{\omega}^{3/2}\Gamma, \quad \tilde{\alpha} = \varepsilon 2\tilde{\omega}\alpha,$$

with all other parameters of order one, one finds that (this consistency condition has not been set explicitly in previous publications) provided

$$\delta \ll \varepsilon \ll 1,$$

the leading order term in  $\delta$ ,  $B(X,T)=B_0(X,T)$ , satisfies the following forced and damped NLS equation (3) with  $\Omega^2=1$ :

$$-iB_T + B_{XX} + (|B|^2 - 1)B = i\varepsilon(\alpha B - \Lambda B_{XX} + \Gamma). \quad (C3)$$

<sup>1</sup>G. Haller, *Chaos Near Resonance*, Applied Mathematical Sciences, Vol. 138 (Springer, New York, 1999).

<sup>2</sup>J. Moloney and A. Newell, *Nonlinear Optics* (Westview, Advanced Book Program, Boulder, CO, 2004).

<sup>3</sup>A. Bishop, M. Forest, D. McLaughlin, and E. Overman II, "A quasi-periodic route to chaos in a near-integrable PDE," *Physica D* **23**, 293–328 (1986).

<sup>4</sup>A. R. Bishop and P. S. Lomdahl, "Nonlinear dynamics in driven, damped sine–Gordon systems," *Physica D* **18**, 54–66 (1986); *Solitons and Coherent Structures* (Santa Barbara, CA, 1985).

<sup>5</sup>A. Bishop, M. Forest, D. McLaughlin, and E. Overman II, "A model representation of chaotic attractors for the driven, damped pendulum chain," *Phys. Lett. A* **144**, 17–25 (1990).

<sup>6</sup>A. Bishop, R. Flesch, M. Forest, D. McLaughlin, and E. Overman II, "Correlations between chaos in a perturbed sine–Gordon equation and a truncated model system," *SIAM J. Math. Anal.* **21**, 1511–1536 (1990).

<sup>7</sup>S. Bishop and M. Clifford, "The use of manifold tangencies to predict orbits, bifurcations, and estimate escape in driven systems," *Chaos, Solitons Fractals* **7**, 1537–1553 (1996).

<sup>8</sup>A. Bishop, D. McLaughlin, M. Forest, and E. I. Overman, "Quasi-periodic route to chaos in a near-integrable PDE: Homoclinic crossings," *Phys. Lett. A* **127**, 335–340 (1988).

<sup>9</sup>A. R. Bishop, K. Fessler, P. S. Lomdahl, W. C. Kerr, M. B. Williams, and S. E. Trullinger, "Coherent spatial structure versus time chaos in a perturbed sine–Gordon system," *Phys. Rev. Lett.* **50**, 1095 (1983).

<sup>10</sup>D. Cai, D. W. McLaughlin, and K. T. R. McLaughlin, "The nonlinear Schrödinger equation as both a PDE and a dynamical system," in *Handbook of Dynamical Systems* (North-Holland, Amsterdam, 2002), Vol. 2, pp. 599–675.

<sup>11</sup>G. Kovacic, "Singular perturbation theory for homoclinic orbits in a class of near-integrable dissipative systems," *J. Dyn. Differ. Equ.* **5**, 559–597 (1993).

<sup>12</sup>G. Haller and S. Wiggins, "Multi-pulse jumping orbits and homoclinic trees in a modal truncation of the damped-forced nonlinear Schrödinger equation," *Physica D* **85**, 311–347 (1995).

<sup>13</sup>G. Haller and S. Wiggins, "N-pulse homoclinic orbits in perturbations of resonant Hamiltonian systems," *Arch. Ration. Mech. Anal.* **130**, 25–101 (1995). Communicated by P. Holmes.

<sup>14</sup>G. Kovacic and S. Wiggins, "Orbits homoclinic to resonances, with an application to chaos in a model of the forced and damped sine–Gordon equation," *Physica D* **57**, 185–225 (1992).

<sup>15</sup>D. W. McLaughlin and J. Shatah, "Homoclinic orbits for PDE's," in *Recent Advances in Partial Differential Equations, Venice 1996*, Proc. Sym-

pos. Appl. Math., Vol. 54 (American Mathematic Society, Providence, RI, 1998), pp. 281–299.

<sup>16</sup>J. Shatah and C. Zeng, "Orbits homoclinic to centre manifolds of conservative PDEs," *Nonlinearity* **16**, 591–614 (2003).

<sup>17</sup>A. Litvak-Hinzenon and V. Rom-Kedar, "Resonant tori and instabilities in Hamiltonian systems," *Nonlinearity* **15**, 1149–1177 (2002).

<sup>18</sup>J. Hanson, J. Cary, and J. Meiss, "Algebraic decay in self-similar Markov chains," *J. Stat. Phys.* **39**, 27–345 (1985).

<sup>19</sup>G. M. Zaslavsky, "Chaos, fractional kinetics, and anomalous transport," *Phys. Rep.* **371**, 461–580 (2002).

<sup>20</sup>J. Meiss, "Symplectic maps, variational principles, and transport," *Rev. Mod. Phys.* **64**, 795–848 (1992).

<sup>21</sup>V. Rom-Kedar, "Homoclinic tangles—classification and applications," *Nonlinearity* **7**, 441–473 (1994).

<sup>22</sup>N. Nekhoroshev, "An exponential estimate of the time of stability of near-integrable Hamiltonian systems," *Russ. Math. Surveys* **32**, 1–65 (1977).

<sup>23</sup>A. Giorgilli, A. Delshams, E. Fontich, L. Galgani, and C. Simó, "Effective stability for Hamiltonian systems near an elliptic point, with an application to the restricted three-body problem," *J. Diff. Eqns.* **77**, 167 (1989).

<sup>24</sup>S. Smale, "Topology and mechanics. I," *Invent. Math.* **10**, 305–331 (1970).

<sup>25</sup>L. M. Lerman and Y. L. Umyskiy, *Four-dimensional Integrable Hamiltonian Systems with Simple Singular Points (Topological Aspects)*, Translations of Mathematical Monographs, Vol. 176 (American Mathematical Society, Providence, RI, 1998). [Translated from the Russian manuscript by A. Kononenko and A. Semenovich.]

<sup>26</sup>R. Abraham and J. E. Marsden, *Foundations of Mechanics* (Benjamin/Cummings, Advanced Book Program, Reading, MA, 1978). Second edition, revised and enlarged, with the assistance of T. Ratiu and R. Cushman.

<sup>27</sup>V. I. Arnol'd, *Dynamical Systems III*, Encyclopedia of Mathematical Sciences Vol. 3, 2nd ed. (Springer, Berlin, 1993).

<sup>28</sup>H. R. Dullin, P. H. Richter, and A. P. Veselov, "Action variables of the Kovalevskaya top," *Regular Chaotic Dyn.* **3**, 18–26 (1998).

<sup>29</sup>*Topological Classification of Integrable Systems*, Advances in Soviet Mathematics, Vol. 6, edited by A. T. Fomenko (American Mathematical Society, Providence, RI, 1991). [Translated from the Russian.]

<sup>30</sup>R. H. Cushman and L. M. Bates, *Global Aspects of Classical Integrable Systems* (Birkhauser, Boston, 1997).

<sup>31</sup>A. V. Bolsinov, "Methods of calculation of the Fomenko–Zieschang invariant," in *Topological Classification of Integrable Systems*, Adv. Soviet Math, Vol. 6 (American Mathematical Society, Providence, RI, 1991), pp. 147–183.

<sup>32</sup>A. Litvak-Hinzenon and V. Rom-Kedar, "Parabolic resonances in 3 degree of freedom near-integrable Hamiltonian systems," *Physica D* **164**, 213–250 (2002).

<sup>33</sup>A. Litvak-Hinzenon and V. Rom-Kedar, "On energy surfaces and the resonance web," *SIAM J. Appl. Dyn. Syst.* (in press).

<sup>34</sup>V. Rom-Kedar, Y. Dvorkin, and N. Paldor, "Chaotic Hamiltonian dynamics of particle's horizontal motion in the atmosphere," *Physica D* **106**, 389–431 (1997).

<sup>35</sup>V. Rom-Kedar, "Parabolic resonances and instabilities," *Chaos* **7**, 148–158 (1997).

<sup>36</sup>N. Lebovitz and A. Pesci, "Dynamics bifurcation in Hamiltonian systems with one degree of freedom," *SIAM (Soc. Ind. Appl. Math.) J. Appl. Math.* **55**, 1117–1133 (1995).

<sup>37</sup>N. N. Nekhoroshev, "Action-angle variables, and their generalizations," *Trans. Mosc. Math. Soc.* **26**, 181–198 (1972).

<sup>38</sup>A. Katok and B. Hasselblatt, *Introduction to the Modern Theory of Dynamical Systems*, Encyclopedia of Mathematics and its Applications, Vol. 54 (Cambridge University Press, Cambridge, 1995).

<sup>39</sup>S. V. Bolotin and D. V. Treschev, "Remarks on the definition of hyperbolic tori of Hamiltonian systems," *Regular Chaotic Dyn.* **5**, 401–412 (2000).

<sup>40</sup>J. Pöschel, "On elliptic lower dimensional tori in Hamiltonian systems," *Math. Z.* **202**, 559–608 (1989).

<sup>41</sup>H. W. Broer, G. B. Huitema, and M. B. Sevryuk, *Quasi-periodic Tori in Families of Dynamical Systems: Order Amidst Chaos*, LNM, Vol. 1645 (Springer, Berlin, 1996).

<sup>42</sup>A. I. Neishtadt, "Passage through a separatrix in a resonance problem with a slowly varying parameter," *Prikl. Mat. Mekh.* **39**, 1331–1334 (1975).